Published December 20, 2010

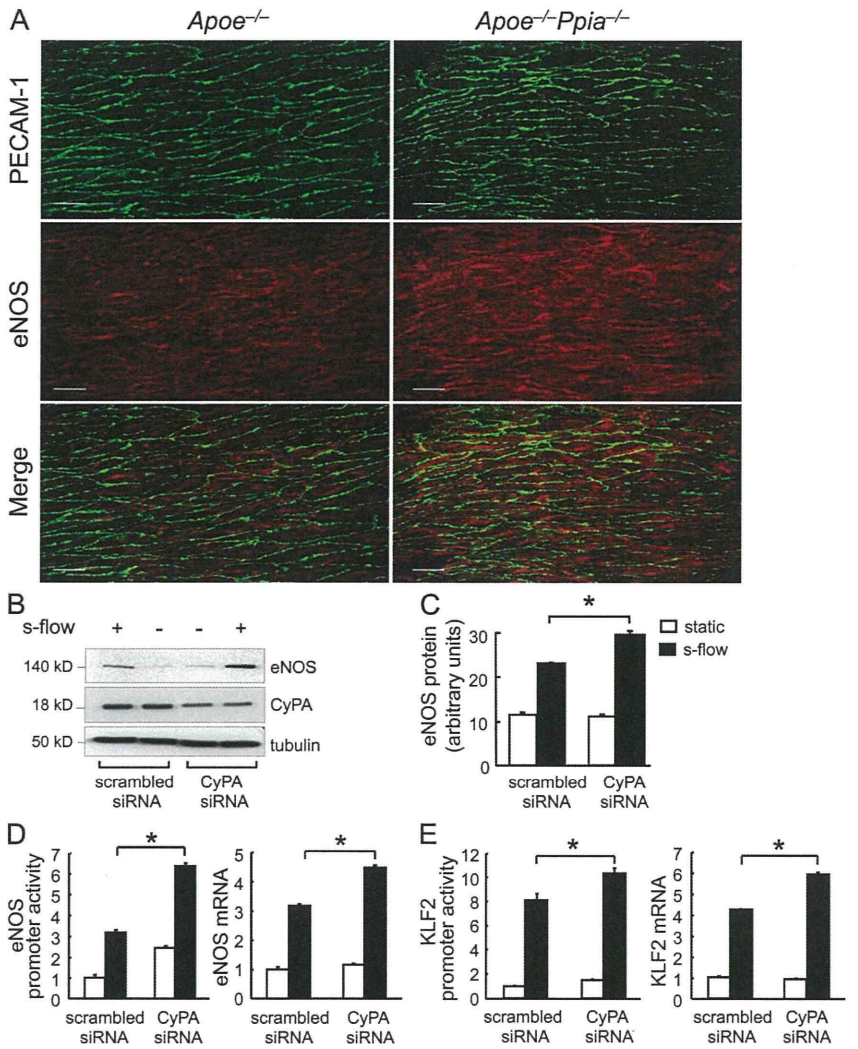

Figure 6. CyPA deficiency and s-flow are associated with increased eNOS expression. (A) Aortas from 12-wk *Apoe*$^{-/-}$ and *Apoe*$^{-/-}$*Ppia*$^{-/-}$ mice were harvested for qualitative analysis of eNOS expression (Alexa Fluor 546; red) by en face dual staining immunofluorescence. PECAM-1 staining (Alexa Fluor 488; green) was used to identify the EC layer. Note that these images were obtained from the thoracic aorta, a region of s-flow. eNOS protein expression was higher in *Apoe*$^{-/-}$*Ppia*$^{-/-}$ mice compared with *Apoe*$^{-/-}$ mice aortas (relative fluorescence of 147 ± 18.48 in *Apoe*$^{-/-}$*Ppia*$^{-/-}$ vs. 100 ± 13.61 in *Apoe*$^{-/-}$; $n = 3$ each group). Bars, 10 µm. (B and C) HUVECs were transfected with CyPA siRNA or scrambled siRNA for 48 h as described in Materials and methods and then exposed to s-flow for 24 h. Western blot analysis shows significantly greater eNOS expression after depletion of CyPA. (D and E) HUVECs were treated for 48 h with CyPA siRNA or scrambled siRNA and then transfected with eNOS (D) or KLF2 (E) promoter. Cells were then exposed to s-flow or maintained in static condition. To evaluate the promoter function, luciferase activity was measured after 24 h. To measure eNOS and KLF2 mRNA levels, a quantitative PCR analysis was performed. (C–E) Results are mean ± SD of three independent experiments performed in triplicate. *, $P < 0.01$ versus scrambled siRNA.

CyPA small interfering RNA (siRNA). Also, CyPA knockdown in HUVECs increased eNOS promoter activity and eNOS messenger RNA (mRNA) levels (Fig. 6 D). Parmar et al. (2006) have shown that the s-flow induction of the KLF2 (Kruppel-like factor 2) transcription factor stimulates eNOS mRNA expression through the ERK5–MEF2–KLF2 pathway. Therefore, we examined whether CyPA could regulate KLF2 expression. As expected, s-flow increased KLF2 promoter activity and KLF2 mRNA levels (Fig. 6 E). These effects were significantly increased by CyPA knockdown. To further substantiate the role of CyPA in the regulation of eNOS expression, we transfected HUVECs with WT CyPA (CyPA-WT). Overexpression of CyPA was accompanied by down-regulation of eNOS at protein (Fig. 7, A and B) and mRNA levels (Fig. 7 C). Consistent with the expression data, overexpression of CyPA decreased eNOS promoter activity in HUVECs (Fig. 7 D). Finally, overexpression of CyPA decreased KLF2 promoter activity (Fig. 7 E) and mRNA levels in HUVECs (Fig. 7 F). These findings illustrate a novel mechanism by which CyPA promotes atherosclerosis, through suppression of KLF2 expression and consequent repression of eNOS transcription.

CyPA affects eNOS expression by a ROS-dependent mechanism

ROS are key mediators of signaling pathways that underlie vascular inflammation in atherogenesis. We have previously shown that CyPA is a key determinant for ROS generation, contributing to the onset of vascular inflammation during aortic aneurism formation (Satoh et al., 2009). Therefore, we evaluated whether ROS are downstream mediators of CyPA in the pathophysiologic context of inflammation we observed. We first overexpressed CyPA in ECs, and then we evaluated the basal level of ROS by dichlorofluorescein (DCF; Fig. 8 A) and dihydroethidium (DHE; Fig. 8 B) staining. ROS production was significantly higher in ECs overexpressing CyPA compared with cells transfected with the vector control (4.2- and 1.6-fold increase in DCF and DHE fluorescence, respectively). These data suggest that CyPA plays a critical role in ROS generation in ECs similar to our findings in VSMCs (Satoh et al., 2009).

Published December 20, 2010

To demonstrate that ROS are key determinants in CyPA-mediated inflammation, we evaluated whether CyPA decreases eNOS expression by a ROS-dependent mechanism. Both the antioxidants *N*-acetyl-cysteine and Tiron, by rebalancing excessive ROS production induced by CyPA overexpression, reversed the CyPA-mediated inhibition of eNOS (Fig. 8 C) and KLF2 promoter activity (Fig. 8 D). These data demonstrated that CyPA induces inflammation through ROS-dependent mechanisms. Based on these results, we believe that CyPA, acting as a proinflammatory cytokine, synergistically augments ROS production, contributing to vascular inflammation and atherogenesis.

Deletion of CyPA decreases EC apoptosis

To ascertain whether intracellular CyPA may participate in the EC apoptosis, we knocked down CyPA in bovine aortic ECs (BAECs) by siRNA and measured hypodiploidia (sub-G_1 cell count) after treatment with TNF plus cycloheximide (CHX) as apoptogens. TNF promoted 11.95 ± 0.07% cell death in cells transfected with scrambled siRNA, and this effect was significantly decreased to 6.65 ± 0.07% by using CyPA siRNA (Fig. 9 A). To better discriminate between apoptosis and necrosis (sub-G_1 cell count might also include necrotic cells), we performed the double staining with annexin V (FITC) and propidium iodide (PI), followed by flow cytometry analysis. Representative cytograms in Fig. 9 B show that cells transfected with scrambled siRNA and treated with TNF plus CHX increased both the percentage of cells gated in the top right quadrant (annexin$^+$/PI$^+$; late apoptotic/necrotic cells) and in the bottom right quadrant (annexin$^+$/PI$^-$; early apoptosis). Transfection of CyPA siRNA significantly attenuated this effect. Moreover, ECs lacking CyPA showed less cleaved caspase-3 expression by Western blot analysis (Fig. 9 C). Because EC apoptosis has been suggested as an initial step in atherogenesis, we studied EC apoptosis in the early stages of the lesion development in mice fed with a high-cholesterol diet for only 1 mo. As shown in Fig. 9 (D and E), there was a marked decrease in apoptotic ECs (detected by terminal deoxynucleotidyl transferase dUTP nick end labeling [TUNEL] staining) in aortic lesions from *Apoe*$^{-/-}$*Ppia*$^{-/-}$ mice compared with littermate control mice. These data underline the crucial role of CyPA during the apoptotic process that is an important early event for the development of atherosclerosis.

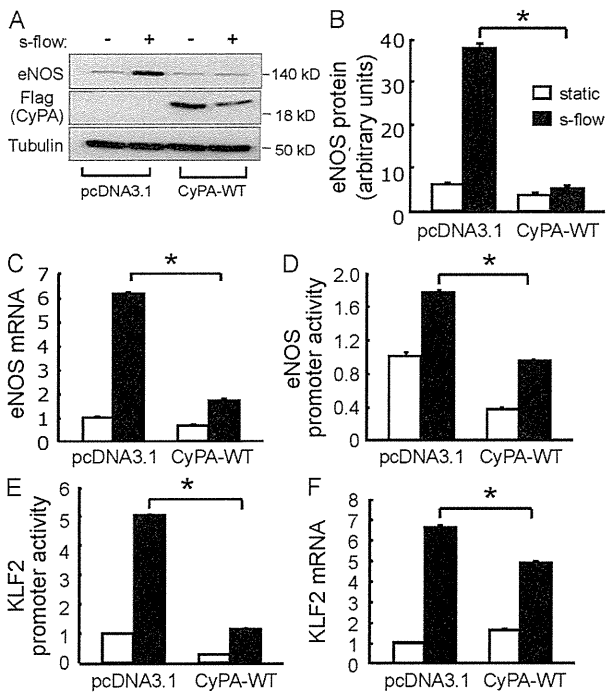

Figure 7. CyPA overexpression decreases eNOS and KLF2 expression. (A) HUVECs were transfected with CyPA-WT for 24 h and then exposed to static and s-flow condition for a further 24 h. (A–F) Western blot data and quantitative PCR analysis revealed that CyPA overexpression inhibited s-flow–induced eNOS protein (A and B), eNOS mRNA (C), and also KLF2 mRNA (F) levels. HUVECs were cotransfected with CyPA-WT and with either eNOS (D) or KLF2 (E) promoter. The cells were exposed to static or s-flow condition, and the luciferase activity was measured after 24 h. Overexpression of CyPA decreases eNOS and KLF2 promoter activity. Data are the mean values ± SD of three independent experiments performed in triplicate. *, P < 0.01 versus control pcDNA3.1.

DISCUSSION

The major finding of this study is that CyPA deficiency in vivo decreases atherosclerotic lesion burden in a mouse model of atherosclerosis. We characterized five important pathological mechanisms by which vascular CyPA promotes atherosclerosis. First, CyPA increases LDL uptake in the vessel wall by regulating the expression of scavenger receptors. Second, CyPA increases EC activation and inflammation by increasing VCAM-1 expression. Third, CyPA decreases eNOS expression through KLF2 transcriptional repression. Fourth, CyPA is a key determinant for TNF-induced EC apoptosis. Finally, CyPA stimulates recruitment of inflammatory cells derived from the BM to the aortic wall. All of these mechanisms, while promoting an environment of oxidative stress, are likely to contribute to the increased atherosclerosis observed in the *Apoe*$^{-/-}$*Ppia*$^{+/+}$ mice.

The decrease in Oil red O staining is consistent with the decrease of multiple lipid uptake receptors in vessels of *Apoe*$^{-/-}$*Ppia*$^{-/-}$ mice. It is likely that CyPA regulates scavenger receptor expression by multiple mechanisms. Because CyPA is a chaperone protein, it may be necessary for appropriate folding and/or transport of LOX-1 and CD36 to the cell membrane. CD36 is mainly expressed in caveolae, and CyPA is essential for caveolae formation via transport of cholesterol and caveolin-1 (Uittenbogaard et al., 1998; Everson and Smart, 2001). In addition, both LOX-1 and CD36 are highly regulated by ROS and cytokines, which are markedly reduced in the *Apoe*$^{-/-}$*Ppia*$^{-/-}$ mice.

The decrease in VCAM-1 expression and increase in eNOS expression observed in *Apoe*$^{-/-}$*Ppia*$^{-/-}$ mice likely contributes to less inflammation. The decrease in VCAM-1

Published December 20, 2010

may be causally related to increased eNOS expression because it was previously shown that eNOS can down-regulate VCAM-1 expression (Kawashima et al., 2001). Consequently, there will be reduced monocyte adhesion to the endothelium, transmigration into the subendothelial space, and inflammation. It may be relevant to note that VCAM-1 expression appears to precede lesion formation (Nakashima et al., 1998; Cybulsky et al., 2001), suggesting an important role for CyPA in the initiation of atherosclerotic lesions. Moreover, we found that CyPA decreased eNOS expression by repressing KLF2 at the transcriptional level. This finding is of significant interest because KLF2 is a central regulator of EC biology (Atkins and Jain, 2007), and it has recently been shown that hemizygous deficiency of KLF2 increased high-cholesterol diet–induced atherosclerosis in *Apoe*$^{-/-}$ mice (Atkins et al., 2008). KLF2 also protects ECs from oxidative stress–mediated injury and subsequent apoptosis (Parmar et al., 2006). The mechanism by which CyPA negatively regulated KLF2 function remains to be elucidated, although a nuclear function for CyPA has been suggested for CXCR4 signaling (Pan et al., 2008).

An essential role for CyPA in apoptosis has become increasingly apparent. We showed that extracellular CyPA promoted EC apoptosis in association with increased JNK (c-Jun N-terminal kinase) and p38 activities (Jin et al., 2004). In this study, we found that knockdown of CyPA in ECs reduced TNF-induced apoptosis in vitro, and CyPA deficiency was associated with a marked decrease in EC apoptosis in early stages of atherosclerosis. A likely mechanism for CyPA-mediated apoptosis is binding and nuclear translocation of AIF (Zhu et al., 2007). In addition, the increase in the vascular oxidative stress requires CyPA (Satoh et al., 2009) and thereby sensitizes ECs to apoptosis.

CyPA may play an important role in several stages of atherosclerosis. During fatty streak formation, it may play a role in lipid uptake via its effect on scavenger receptors. In all

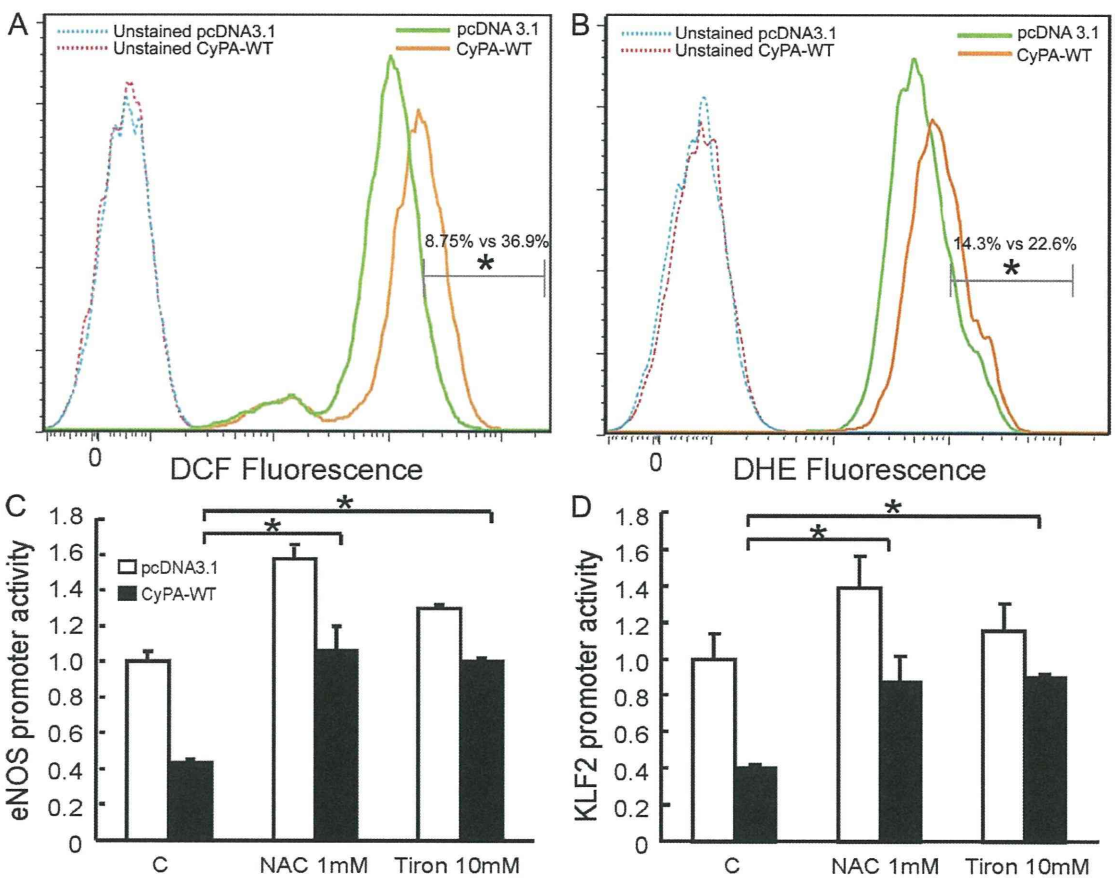

Figure 8. CyPA increases ROS levels in ECs. (A and B) HUVECs were transfected with CyPA-WT and vector control. After 48 h of incubation, ROS levels were measured by determining DCF (A) and DHE (B) fluorescence. CyPA overexpression significantly increased ROS content in cells. Data are the representation of three independent experiments performed in triplicate. *, $P < 0.01$ vs. control pcDNA3.1. (C and D) HUVECs were transfected with CyPA-WT and vector control. After 24 h, cells were treated with 1 mM *N*-acetyl-cysteine and 10 mM Tiron. 16 h later, eNOS (C) and KLF2 (D) promoter activity were measured by luciferase assay. Data are the mean values ± SD of three independent experiments performed in triplicate. *, $P < 0.01$ versus control pcDNA3.1.

Published December 20, 2010

stages, it may play a role in inflammation by promoting monocyte adhesion and recruitment as well as contributing to an oxidative environment. The data from Seizer et al. (2010) showing that CyPA is secreted from foam cells suggest an important role in later stages of atherosclerosis. Finally, we have recently shown an essential role for CyPA for matrix metalloproteinase activation (Satoh et al., 2009), suggesting that CyPA may also play an important role in plaque rupture. Altogether, our data suggest that the agents that inhibit CyPA expression or agents that block CyPA receptors might be candidates that may regulate atherosclerotic plaque and its rupture.

We would like to point out that studies in animals and humans, although contradictory and not conclusive, have reported that CsA, the immunosuppressive drug that inhibits CyPA, increases hyperlipidemia and risk of atherosclerosis (Fernández-Miranda et al., 1998; Ojo, 2006; Kockx et al., 2010). We also reported that decreasing cholesterol content in caveolae by CsA is a potentially important pathogenic mechanism for CsA-induced endothelial dysfunction and atherosclerosis (Lungu et al., 2004). These findings appear to contradict our data. However, the diversity of the pathways affected by CsA does not allow for simple conclusions to be drawn. CsA also affects many cellular pathways not associated

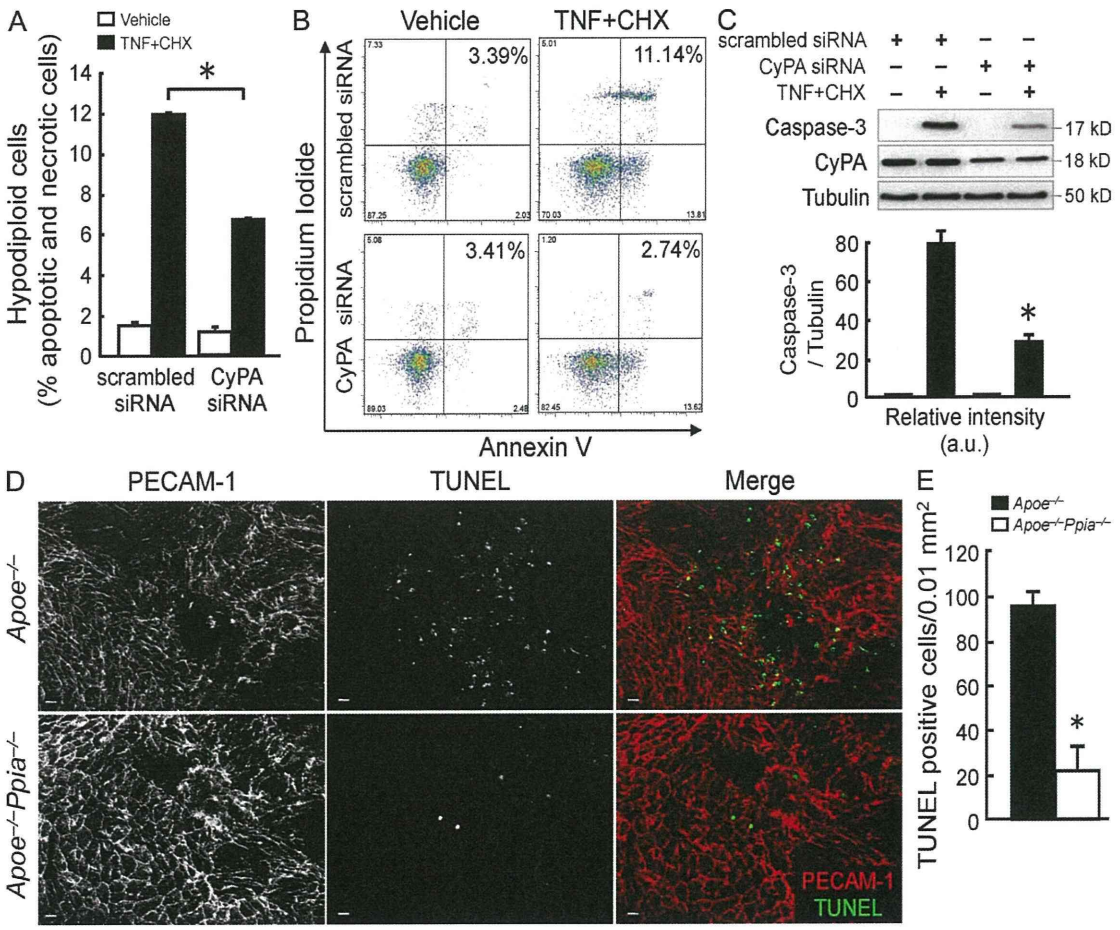

Figure 9. CyPA deficiency reduces EC apoptosis in vitro and in vivo. (A) BAECs were transfected with CyPA siRNA or scrambled siRNA for 48 h and then treated with 10 ng/ml TNF + 10 µg/ml CHX for 6 h. Apoptotic cells were determined by their hypochromic, subdiploid staining profiles (sub-G_1 population). The data represent the mean ± SD of triplicate samples repeated in three separate experiments. *, $P < 0.01$ versus scrambled siRNA. (B) Dot-plot diagrams of FITC-conjugated annexin V– and PI-stained cells after treatment with TNF + CHX for 3 h. Results are representative of two separate experiments that gave similar results. (C) Western blot analyses of cleaved caspase-3 in BAECs treated with TNF + CHX for 6 h. Data represent the mean ± SD of three separate experiments. *, $P < 0.01$ versus scrambled siRNA. (D) Whole-mount en face dual immunofluorescence staining of *Apoe*$^{-/-}$ and *Apoe*$^{-/-}$*Ppia*$^{-/-}$ mice aortas after 4 wk of a high-cholesterol diet. Note that these images were obtained from the inner curvature of the aortic arch, which is a region of disturbed flow. PECAM-1 staining shows polygonal ECs that are not aligned with flow. TUNEL staining shows increased fluorescence in *Apoe*$^{-/-}$ mice. Bars, 10 µm. (E) Quantitative data show that *Apoe*$^{-/-}$*Ppia*$^{-/-}$ mice aortas have a significant decrease in apoptotic cells in the lesion area. The data are expressed as the percentage of TUNEL-positive cells per field (four fields per three mice each group). *, $P < 0.01$ compared with *Apoe*$^{-/-}$ mice. Results are the mean ± SD and show pooled data from two experiments.

Published December 20, 2010

with immunosuppression, several of which can be linked to its cardiovascular side effects. Moreover, CsA is not a selective drug for CyPA. In fact, CyPA, -B, and -C all bind with high affinity to CsA in vitro (Bram et al., 1993). Therefore, the proatherogenic effect of CsA could be related to the inhibition of other cyclophilin isoforms. In addition, CsA could promote atherosclerosis by a CyPA-independent mechanism. For example, CsA directly binds to LDL and affects LDL metabolism at several levels (López-Miranda et al., 1993; Vaziri et al., 2000). We believe that the discovery of more uniquely selective and specific inhibitors of CyPA will be a good therapeutic approach for atherosclerosis.

MATERIALS AND METHODS

Animal procedures. All animal experiments were conducted in accordance with experimental protocols that were approved by the University Committee on Animal Resources at the University of Rochester. *Ppia*$^{-/-}$ mice were purchased from The Jackson Laboratory and were backcrossed to C57BL/6J mice for 10 generations. The *Apoe*$^{-/-}$ mice on a C57BL/6J background were obtained from The Jackson Laboratory. Double knockout *Apoe*$^{-/-}$*Ppia*$^{-/-}$ mice were generated by crossing *Ppia*$^{-/-}$ mice with *Apoe*$^{-/-}$ mice. The F1 generation was backcrossed with *Apoe*$^{-/-}$ mice to fix the *Apoe*$^{-/-}$ genotype, and littermates were crossed. All mice were genotyped by PCR on tail clip samples, and all experiments were performed with generations F4–F6 using littermate *Apoe*$^{-/-}$*Ppia*$^{+/+}$ as controls. Animals were housed under a 12-h light and 12-h dark regimen. Accelerated atherosclerosis was induced by feeding the mice for 16 wk with a high-cholesterol diet containing 1.25% cholesterol (Research Diets D12108C).

Atherosclerotic lesion analysis. Mice were anesthetized with an intraperitoneal injection of 80 mg kg^{-1} ketamine and 5 mg kg^{-1} xylazine. Hearts were perfused through the left ventricle with PBS followed by 10% buffered formaldehyde. After fixation overnight in 10% formaldehyde, the aortas were thoroughly cleaned under a dissecting microscope. All adventitial fat and connective tissue was carefully removed. The vessels were then cut open longitudinally through the inner curvature and the ventral portions of the thoracic and abdominal sections. Aortas were rinsed with 5 ml of 60% isopropanol for 5 min. Staining was performed with 5 ml of filtered Oil red O solution (Poly Scientific) for 15 min. Vessels were then rinsed with 60% isopropanol for 15 min, followed by a final rinse with distilled water. After staining, the greater curvature of the aorta was cut to divide the arch in half. The vessel was precisely pinned to black wax in PBS to reveal the entire luminal surface area. Images were obtained using SPOT version 4.1.1, a camera (SPOT Insight 4; Diagnostic Instruments, Inc.) connected to a microscope (MZ12.5; Leica). Plaques were analyzed in Photoshop 8.0 (Adobe), and lesion area was quantified using Image-Pro Analyzer 6.2 (Media Cybernetics).

Histological analysis. Mice were anesthetized and euthanized. For morphological analysis, aortas were perfused with normal saline and fixed with 10% phosphate-buffered formalin at physiological pressure for 5 min (Satoh et al., 2008). The whole aortas and hearts were harvested, fixed for 24 h, and embedded in paraffin, and 5-µm cross sections were prepared. Paraffin sections were stained with H&E or Masson and Trichrome or used for immunostaining. Analyses were performed by using Image-Pro Plus software (Media Cybernetics).

Immunohistochemistry. Formaldehyde-fixed paraffin sections were incubated with primary antibody overnight at 4°C. The primary antibodies used were Mac3 (clone M3/84; 1:200 dilution; BD) and α-smooth muscle actin (clone 1A4; 1:1,000 dilution; Sigma-Aldrich). As a negative control, species- and isotype-matched IgG were used in place of the primary antibody. Slides were viewed with a microscope (BX41; Olympus) and with digital camera (SPOT Insight 2; Diagnostic Instruments, Inc.). Vessel areas and densitometric analysis were measured with Image-Pro Plus software.

En face analysis. Immunofluorescence staining of mouse aortic ECs was performed as described previously (Won et al., 2007). Aortas were perfused with PBS followed by 2% paraformaldehyde for 10 min. After fixation, the aortas were cut in small segments and incubated in blocking buffer containing 2% BSA. Primary antibody incubations were performed overnight at 4°C. The primary antibodies used were VCAM-1 (1:200; Santa Cruz Biotechnology, Inc.), eNOS (1:100; BD), and PECAM-1 (1:200; BD). After washing the aortic segments three times, secondary antibodies were added and incubated for 1 h. Negative controls included addition of nonimmune goat or rabbit IgG. After washing, aortic specimens were opened, placed on a glass slide with the luminal side up, and then mounted for confocal microscopy (FLUOVIEW; Olympus).

Ex vivo LDL tissue uptake. *Apoe*$^{-/-}$ and *Apoe*$^{-/-}$*Ppia*$^{-/-}$ mice were anesthetized and euthanized. Aortas were dissected, cut in small fragments, and incubated in 50 µg/ml DiI-LDL. After 2 h, aortas were washed with PBS and fixed using 4% paraformaldehyde. Then, aortic segments were opened and stained with SYTOX green nucleic acid stain (dilution 1:10,000; Invitrogen). After washing, the aortic specimens were prepared for en face analysis by confocal microscopy (FLUOVIEW). Analysis of different images was performed using Image-Pro Plus software. The results are expressed in terms of fluorescence-positive areas for each animal (n = 3 each group, 4 fields each animal). Human LDL was isolated by ultracentrifugation (1.019 g/ml < d < 1.063 g/ml) and dialyzed against 0.15 M NaCl/1 mM EDTA overnight at 4°C using a 50,000 MWCO dialysis membrane. The LDL (250 µg) was directly iodinated using iodobeads (Thermo Fisher Scientific) as described by the manufacturer, and unincorporated ^{125}I was removed by two rounds of gel filtration on PD10 columns (GE Healthcare) using PBS, pH 7.0, as elution buffer. The ^{125}I-labeled LDL was adjusted to a specific activity of 500 dpm/ng by addition of unlabeled LDL and then filter sterilized using 0.2 µm Acrodisk syringe filter (Pall Life Sciences). More than 98% of the radioactivity in the [^{125}I]LDL preparation was precipitable with trichloroacetic acid. For [^{125}I]LDL uptake experiments, aortas (n = 4 each group) were incubated with 10 µg/ml [^{125}I]LDL in serum-free medium. After a 3-h incubation at 37°C, aortas were washed three times with 2 ml PBS and assayed for cell-associated label and protein content (Podrez et al., 1999). Measurement of radioactivity was performed in a gamma counter (Wallac 1470 Automatic Gamma Counter; EG&G Wallac).

Western blot analysis. Aortic tissue samples were frozen with liquid nitrogen, crushed, and lysed in cell lysis buffer (Cell Signaling Technology) with protease inhibitor cocktail (Sigma-Aldrich). HUVECs and BAECs were washed twice with PBS and harvested on ice in radioimmunoprecipitation assay lysis buffer (50 mmol/l Hepes, 10 mmol/l EDTA, 150 mmol/l NaCl, 1% NP-40, 0.5% Na deoxycholate, and 0.1% SDS, pH 7.4) supplemented with the protease inhibitor cocktail. Total cell lysates were loaded on SDS-PAGE and electrotransferred into nitrocellulose membrane followed by blocking 1 h at room temperature in 5% nonfat dry milk in PBS/0.1% Tween 20. After being washed three times with PBS/0.1% Tween 20, the blots were incubated overnight at 4°C with the appropriate primary antibody. The primary antibodies used were CyPA (1:5,000 dilution; Enzo Life Sciences, Inc.), LOX-1 (1:1,000 dilution; Abcam), SR-BI (1:1,000 dilution; Abcam), CD36 (1:1,000 dilution; Santa Cruz Biotechnology, Inc.), VCAM-1 (1:2,000 dilution; Santa Cruz Biotechnology, Inc.), actin (1:5,000 dilution; Santa Cruz Biotechnology, Inc.), eNOS (1:1,000 dilution; BD), α-tubulin (1:5,000 dilution; Sigma-Aldrich), Flag (1:2,000 dilution; Sigma-Aldrich), and caspase-3 (1:1,000 dilution; Cell Signaling Technology). ApoB isoforms present in serum were determined by immunoblotting with rabbit anti–rat apoB antibodies prepared in our laboratory (Chirieac et al., 2000). The membranes were incubated with peroxidase-conjugated secondary antibodies for 1 h. Signals were visualized using the enhanced chemiluminescence Western blotting detection system (GE Healthcare). Images were acquired with a

Published December 20, 2010

JEM

Gel Doc system (Gel Doc 2000; Bio-Rad Laboratories), and a densitometric analysis of membranes was performed using the Bio-Rad Laboratories software.

Lipids analysis and lipoprotein profiles measurement. Mice were anesthetized, and blood samples were collected from the left ventricle. Plasma was prepared and stored at −80°C. Plasma cholesterol and triglycerides were enzymatically measured using the Cholesterol E kit (Wako Chemicals USA, Inc.) and Infinity Triglyceride kit (Thermo Fisher Scientific), respectively, according to the manufacturers' instructions. Lipoproteins in pooled plasma samples (100 µl) from nine *Apoe*$^{-/-}$ mice and nine *Apoe*$^{-/-}$*Ppia*$^{-/-}$ mice were assessed by fast performance liquid chromatography using a Superose 6 HR 10/30 column (GE Healthcare) at a flow rate of 0.4 ml/min. Cholesterol and triglyceride concentrations were measured in each fraction by the aforementioned methods.

BM transplantation. BM transplantation was performed as described previously (Satoh et al., 2006). In brief, recipient mice were lethally irradiated and received an intravenous injection of 5×10^6 donor BM cells suspended in 100 µl of calcium- and magnesium-free PBS with 2% FBS. After transplantation, the mice were placed on a regular chow diet for 6 wk followed by high-cholesterol diet for 12 wk. Transgenic mice ubiquitously expressing GFP were obtained from The Jackson Laboratory. The chimeric rate assessed by reconstitution with GFP$^+$ BM cells was >99% by FACS analysis (FACSCanto II; BD).

BM-derived cell recruitment assays. Quantitative numbers or percentages of the migrating GFP$^+$ cells was analyzed by en face staining as reported in En face analysis. PECAM-1 antibody was used to identify the EC by using a FLUOVIEW confocal microscope.

Cell culture and transfection. HUVECs were obtained from collagenase-digested umbilical veins and collected in M200 medium supplemented with low serum growth supplement (Invitrogen), 5% fetal calf serum (Invitrogen), 50 U/ml penicillin, and 50 µg/ml streptomycin. BAECs were cultured in M199 medium (Invitrogen) supplemented with 10% fetal clone III (Hyclone), MEM–amino acids, 50 U/ml penicillin, and 50 µg/ml streptomycin. HUVECs as well as BAECs were cultured on 2% gelatin–precoated dishes. For transient expression experiments, 80% confluent cells were transfected using Opti-MEM and Lipofectamine 2000 (Invitrogen). 3 h after transfection, Opti-MEM was replaced with complete media, and cells were exposed to flow 24 h later. For siRNA-driven depletion of CyPA, HUVECs and BAECs were transiently transfected with 100 nM scrambled siRNA or CyPA siRNA using Lipofectamine 2000 reagent. The cells were used 48 h after siRNA transfection.

Steady laminar flow (s-flow) protocol. Confluent cells cultured in 100-mm dishes were exposed to flow in a cone and plate viscometer placed in an incubator with 5% CO_2 at 37°C for 24 h (shear stress = 12 dyn/cm^2).

eNOS and KLF2 promoter activity. HUVECs were transiently cotransfected with human eNOS promoter (provided by D. Gardner, University of California, San Francisco, San Francisco, CA) or KLF2 promoter (provided by J. Lingrel, University of Cincinnati, Cincinnati, OH) and β-galactosidase using Lipofectamine 2000. After 8 h, the cells were exposed to flow. 24 h later, cells were lysed in passive lysis buffer (Promega). Luciferase assays were performed using the Luciferase assay system (Promega). Luciferase activity was normalized to β-galactosidase activity to correct for differences in transfection efficiency.

Real-time quantitative PCR analysis of eNOS and KLF2. Total RNA was isolated by TRIZOL reagent (Invitrogen), and reverse transcription was conducted by using TaqMan reverse transcription reagents (Applied Biosystems) according to the manufacturer's instructions. The relative quantities of mRNAs were obtained using the comparative Ct method and were normalized by GAPDH (Applied Biosystems).

ROS measurement. The evaluation of ROS production was performed as described previously (Griendling and FitzGerald, 2003). After transfection with CyPA-WT and vector control for 48 h, HUVECs were washed with PBS and loaded with 10 µM 2,7-DCF diacetate (H2DCF-DA; Invitrogen) or 5 µM DHE (Invitrogen) for 30 min at 37°C. ROS levels were measured using flow cytometry (FACSCanto II). Data from 20,000 events per sample were collected, and forward light scatter characteristics were evaluated to exclude cell debris from the analysis.

Apoptosis analysis. Apoptotic cells were determined by analyzing their subdiploid staining profiles (sub-G_1 population). BAECs were cultured in the presence of TNF + CHX and then washed in PBS, resuspended (5×10^5 cells/ml) in PI hypotonic solution (0.1% Na citrate, 0.1% Triton X-100, and 50 µg/ml PI), and left at 4°C for 30 min in the dark. Data from 20,000 events per sample were collected by flow cytometry (FACSCanto II). Forward light scatter characteristics were used so that cell debris could be excluded from the analysis. For the estimation of apoptotic cells, cells were collected and double labeled with FITC-conjugated annexin V and PI according to the manufacturer's instructions (Trevigen). Green (FITC-conjugated annexin V) and red (PI) fluorescence of individual cells were measured by flow cytometry (FACSCanto II). Electronic compensation was required to exclude overlapping of the two emission spectra. For the detection of apoptosis on the whole aortic mount, FITC-labeled dUTP nick end labeling (TUNEL) method was applied to the aortic segments by using an In Situ Apoptosis Detection kit-POD according to the manufacturer's instruction (Roche). Images were acquired by confocal microscopy (FLUOVIEW).

Statistical analyses. Quantitative results are expressed as mean ± SD. Comparisons of parameters among two groups were made by the unpaired Student's *t* test. Comparisons of parameters among the three groups were made by one-way analysis of variance, and comparisons of different parameters between the two genotypes were made by two-way analysis of variance, followed by a post hoc analysis using the Bonferroni test. Statistical significance was evaluated with StatView (StatView 5.0; SAS Institute, Inc.). A value of $P < 0.05$ was considered to be statistically significant.

Online supplemental material. Fig. S1 shows that CyPA deficiency prevents atherosclerosis formation. Fig. S2 shows that CyPA deficiency decreases LDL uptake in the lesser curvature of the mouse aorta. Fig. S3 shows that CyPA regulates LDL uptake. Fig. S4 shows metabolic parameters in the absence of CyPA. Fig. S5 shows that CyPA promotes EC damage and disorganization. Online supplemental material is available at http://www.jem.org/cgi/content/full/jem.20101174/DC1.

We are grateful to the Aab Cardiovascular Research Institute members for useful suggestions and Mary A. Georger, Joanne Cianci, and Chelsea Wong for technical assistance. We are also grateful to Eiichiro Yamamoto for assisting with data analysis.

This work was supported by National Institutes of Health grant HL49192 (to B.C. Berk), Internal Grant of the University of Salerno (to P. Nigro), Japan Heart Foundation/Bayer Yakuhin Research Grant Abroad (to K. Satoh), Japan Heart Foundation/Novartis Grant for Research Award on Molecular and Cellular Cardiology (to K. Satoh), AstraZeneca Research Grant (to K. Satoh), and grants-in-aid from the Japanese Ministry of Education, Culture, Sports, Science and Technology (to K. Satoh).

The authors declare no competing financial interests.

Submitted: 11 June 2010
Accepted: 23 November 2010

REFERENCES

Allain, F., C. Vanpouille, M. Carpentier, M.C. Slomianny, S. Durieux, and G. Spik. 2002. Interaction with glycosaminoglycans is required for cyclophilin B to trigger integrin-mediated adhesion of peripheral blood T lymphocytes to extracellular matrix. *Proc. Natl. Acad. Sci. USA.* 99:2714–2719. doi:10.1073/pnas.052284899

Arora, K., W.M. Gwinn, M.A. Bower, A. Watson, I. Okwumabua, H.R. MacDonald, M.I. Bukrinsky, and S.L. Constant. 2005. Extracellular cyclophilins contribute to the regulation of inflammatory responses. *J. Immunol.* 175:517–522.

Atkins, G.B., and M.K. Jain. 2007. Role of Krüppel-like transcription factors in endothelial biology. *Circ. Res.* 100:1686–1695. doi:10.1161/01.RES.0000267856.00713.0a

Atkins, G.B., Y. Wang, G.H. Mahabeleshwar, H. Shi, H. Gao, D. Kawanami, V. Natesan, Z. Lin, D.I. Simon, and M.K. Jain. 2008. Hemizygous deficiency of Krüppel-like factor 2 augments experimental atherosclerosis. *Circ. Res.* 103:690–693. doi:10.1161/CIRCRESAHA.108.184663

Berk, B.C. 2008. Atheroprotective signaling mechanisms activated by steady laminar flow in endothelial cells. *Circulation.* 117:1082–1089. doi:10.1161/CIRCULATIONAHA.107.720730

Bram, R.J., D.T. Hung, P.K. Martin, S.L. Schreiber, and G.R. Crabtree. 1993. Identification of the immunophilins capable of mediating inhibition of signal transduction by cyclosporin A and FK506: roles of calcineurin binding and cellular location. *Mol. Cell. Biol.* 13:4760–4769.

Chen, J., P.J. Kuhlencordt, J. Astern, R. Gyurko, and P.L. Huang. 2001. Hypertension does not account for the accelerated atherosclerosis and development of aneurysms in male apolipoprotein e/endothelial nitric oxide synthase double knockout mice. *Circulation.* 104:2391–2394. doi:10.1161/hc4501.099729

Chirieac, D.V., L.R. Chirieac, J.P. Corsetti, J. Cianci, C.E. Sparks, and J.D. Sparks. 2000. Glucose-stimulated insulin secretion suppresses hepatic triglyceride-rich lipoprotein and apoB production. *Am. J. Physiol. Endocrinol. Metab.* 279:E1003–E1011.

Colgan, J., M. Asmal, M. Neagu, B. Yu, J. Schneidkraut, Y. Lee, E. Sokolskaja, A. Andreotti, and J. Luban. 2004. Cyclophilin A regulates TCR signal strength in CD4+ T cells via a proline-directed conformational switch in Itk. *Immunity.* 21:189–201. doi:10.1016/j.immuni.2004.07.005

Cybulsky, M.I., and M.A. Gimbrone Jr. 1991. Endothelial expression of a mononuclear leukocyte adhesion molecule during atherogenesis. *Science.* 251:788–791. doi:10.1126/science.1990440

Cybulsky, M.I., K. Iiyama, H. Li, S. Zhu, M. Chen, M. Iiyama, V. Davis, J.C. Gutierrez-Ramos, P.W. Connelly, and D.S. Milstone. 2001. A major role for VCAM-1, but not ICAM-1, in early atherosclerosis. *J. Clin. Invest.* 107:1255–1262. doi:10.1172/JCI11871

Damsker, J.M., M.I. Bukrinsky, and S.L. Constant. 2007. Preferential chemotaxis of activated human CD4+ T cells by extracellular cyclophilin A. *J. Leukoc. Biol.* 82:613–618. doi:10.1189/jlb.0506317

Everson, W.V., and E.J. Smart. 2001. Influence of caveolin, cholesterol, and lipoproteins on nitric oxide synthase: implications for vascular disease. *Trends Cardiovasc. Med.* 11:246–250. doi:10.1016/S1050-1738(01)00119-0

Fernández-Miranda, C., C. Guijarro, A. de la Calle, C. Loinaz, I. Gonzalez-Pinto, T. Gómez-Izquierdo, S. Larumbe, E. Moreno, and A. del Palacio. 1998. Lipid abnormalities in stable liver transplant recipients—effects of cyclosporin, tacrolimus, and steroids. *Transpl. Int.* 11:137–142. doi:10.1111/j.1432-2277.1998.tb00789.x

Galkina, E., and K. Ley. 2009. Immune and inflammatory mechanisms of atherosclerosis (*). *Annu. Rev. Immunol.* 27:165–197. doi:10.1146/annurev.immunol.021908.132620

Glass, C.K., and J.L. Witztum. 2001. Atherosclerosis. The road ahead. *Cell.* 104:503–516. doi:10.1016/S0092-8674(01)00238-0

Griendling, K.K., and G.A. FitzGerald. 2003. Oxidative stress and cardiovascular injury: Part I: basic mechanisms and in vivo monitoring of ROS. *Circulation.* 108:1912–1916. doi:10.1161/01.CIR.0000093660.86242.BB

Handa, S., A.M. Sadi, M.I. Cybulsky, D.J. Stewart, and M. Husain. 2008. Region-specific patterns of vascular remodelling occur early in atherosclerosis and without loss of smooth muscle cell markers. *Atherosclerosis.* 196:617–623. doi:10.1016/j.atherosclerosis.2007.06.032

Handschumacher, R.E., M.W. Harding, J. Rice, R.J. Drugge, and D.W. Speicher. 1984. Cyclophilin: a specific cytosolic binding protein for cyclosporin A. *Science.* 226:544–547. doi:10.1126/science.6238408

Hansson, G.K. 2005. Inflammation, atherosclerosis, and coronary artery disease. *N. Engl. J. Med.* 352:1685–1695. doi:10.1056/NEJMra043430

Hansson, G.K., and P. Libby. 2006. The immune response in atherosclerosis: a double-edged sword. *Nat. Rev. Immunol.* 6:508–519. doi:10.1038/nri1882

Jin, Z.G., M.G. Melaragno, D.F. Liao, C. Yan, J. Haendeler, Y.A. Suh, J.D. Lambeth, and B.C. Berk. 2000. Cyclophilin A is a secreted growth factor induced by oxidative stress. *Circ. Res.* 87:789–796.

Jin, Z.G., A.O. Lungu, L. Xie, M. Wang, C. Wong, and B.C. Berk. 2004. Cyclophilin A is a proinflammatory cytokine that activates endothelial cells. *Arterioscler. Thromb. Vasc. Biol.* 24:1186–1191. doi:10.1161/01.ATV.0000130664.51010.28

Kawashima, S., and M. Yokoyama. 2004. Dysfunction of endothelial nitric oxide synthase and atherosclerosis. *Arterioscler. Thromb. Vasc. Biol.* 24:998–1005. doi:10.1161/01.ATV.0000125114.88079.96

Kawashima, S., T. Yamashita, M. Ozaki, Y. Ohashi, H. Azumi, N. Inoue, K. Hirata, Y. Hayashi, H. Itoh, and M. Yokoyama. 2001. Endothelial NO synthase overexpression inhibits lesion formation in mouse model of vascular remodeling. *Arterioscler. Thromb. Vasc. Biol.* 21:201–207.

Khromykh, L.M., N.L. Kulikova, T.V. Anfalova, T.A. Muranova, V.M. Abramov, A.M. Vasiliev, V.S. Khlebnikov, and D.B. Kazansky. 2007. Cyclophilin A produced by thymocytes regulates the migration of murine bone marrow cells. *Cell. Immunol.* 249:46–53. doi:10.1016/j.cellimm.2007.11.002

Kim, H., W.J. Kim, S.T. Jeon, E.M. Koh, H.S. Cha, K.S. Ahn, and W.H. Lee. 2005. Cyclophilin A may contribute to the inflammatory processes in rheumatoid arthritis through induction of matrix degrading enzymes and inflammatory cytokines from macrophages. *Clin. Immunol.* 116:217–224. doi:10.1016/j.clim.2005.05.004

Knowles, J.W., R.L. Reddick, J.C. Jennette, E.G. Shesely, O. Smithies, and N. Maeda. 2000. Enhanced atherosclerosis and kidney dysfunction in eNOS(−/−)Apoe(−/−) mice are ameliorated by enalapril treatment. *J. Clin. Invest.* 105:451–458. doi:10.1172/JCI8376

Kockx, M., W. Jessup, and L. Kritharides. 2010. Cyclosporin A and atherosclerosis—cellular pathways in atherogenesis. *Pharmacol. Ther.* 128:106–118. doi:10.1016/j.pharmthera.2010.06.001

Kuhlencordt, P.J., R. Gyurko, F. Han, M. Scherrer-Crosbie, T.H. Aretz, R. Hajjar, M.H. Picard, and P.L. Huang. 2001. Accelerated atherosclerosis, aortic aneurysm formation, and ischemic heart disease in apolipoprotein E/endothelial nitric oxide synthase double-knockout mice. *Circulation.* 104:448–454. doi:10.1161/hc2901.091399

Li, H., and U. Förstermann. 2009. Prevention of atherosclerosis by interference with the vascular nitric oxide system. *Curr. Pharm. Des.* 15:3133–3145. doi:10.2174/138161209789058002

Liao, D.F., Z.G. Jin, A.S. Baas, G. Daum, S.P. Gygi, R. Aebersold, and B.C. Berk. 2000. Purification and identification of secreted oxidative stress-induced factors from vascular smooth muscle cells. *J. Biol. Chem.* 275:189–196. doi:10.1074/jbc.275.1.189

López-Miranda, J., E. Vilella, F. Pérez-Jiménez, A. Espino, J.A. Jiménez-Perepérez, L. Masana, and P.R. Turner. 1993. Low-density lipoprotein metabolism in rats treated with cyclosporine. *Metabolism.* 42:678–683. doi:10.1016/0026-0495(93)90232-D

Lungu, A.O., Z.G. Jin, H. Yamawaki, T. Tanimoto, C. Wong, and B.C. Berk. 2004. Cyclosporin A inhibits flow-mediated activation of endothelial nitric-oxide synthase by altering cholesterol content in caveolae. *J. Biol. Chem.* 279:48794–48800. doi:10.1074/jbc.M313897200

Nakashima, Y., A.S. Plump, E.W. Raines, J.L. Breslow, and R. Ross. 1994. ApoE-deficient mice develop lesions of all phases of atherosclerosis throughout the arterial tree. *Arterioscler. Thromb.* 14:133–140.

Nakashima, Y., E.W. Raines, A.S. Plump, J.L. Breslow, and R. Ross. 1998. Upregulation of VCAM-1 and ICAM-1 at atherosclerosis-prone sites on the endothelium in the ApoE-deficient mouse. *Arterioscler. Thromb. Vasc. Biol.* 18:842–851.

Oemar, B.S., M.R. Tschudi, N. Godoy, V. Brovkovich, T. Malinski, and T.F. Lüscher. 1998. Reduced endothelial nitric oxide synthase expression and production in human atherosclerosis. *Circulation.* 97:2494–2498.

Ojo, A.O. 2006. Cardiovascular complications after renal transplantation and their prevention. *Transplantation.* 82:603–611. doi:10.1097/01.tp.0000235527.81917.fe

Pan, H., C. Luo, R. Li, A. Qiao, L. Zhang, M. Mines, A.M. Nyanda, J. Zhang, and G.H. Fan. 2008. Cyclophilin A is required for CXCR4-mediated nuclear export of heterogeneous nuclear ribonucleoprotein A2, activation and nuclear translocation of ERK1/2, and chemotactic cell migration. *J. Biol. Chem.* 283:623–637. doi:10.1074/jbc.M704934200

Parmar, K.M., H.B. Larman, G. Dai, Y. Zhang, E.T. Wang, S.N. Moorthy, J.R. Kratz, Z. Lin, M.K. Jain, M.A. Gimbrone Jr., and G. García-Cardeña. 2006. Integration of flow-dependent endothelial phenotypes by Kruppel-like factor 2. *J. Clin. Invest.* 116:49–58. doi:10.1172/JCI24787

Podrez, E.A., D. Schmitt, H.F. Hoff, and S.L. Hazen. 1999. Myeloperoxidase-generated reactive nitrogen species convert LDL into an atherogenic form in vitro. *J. Clin. Invest.* 103:1547–1560. doi:10.1172/JCI5549

Satoh, K., Y. Kagaya, M. Nakano, Y. Ito, J. Ohta, H. Tada, A. Karibe, N. Minegishi, N. Suzuki, M. Yamamoto, et al. 2006. Important role of endogenous erythropoietin system in recruitment of endothelial progenitor cells in hypoxia-induced pulmonary hypertension in mice. *Circulation.* 113:1442–1450. doi:10.1161/CIRCULATIONAHA.105.583732

Satoh, K., T. Matoba, J. Suzuki, M.R. O'Dell, P. Nigro, Z. Cui, A. Mohan, S. Pan, L. Li, Z.G. Jin, et al. 2008. Cyclophilin A mediates vascular remodeling by promoting inflammation and vascular smooth muscle cell proliferation. *Circulation.* 117:3088–3098. doi:10.1161/CIRCULATIONAHA.107.756106

Satoh, K., P. Nigro, T. Matoba, M.R. O'Dell, Z. Cui, X. Shi, A. Mohan, C. Yan, J. Abe, K.A. Illig, and B.C. Berk. 2009. Cyclophilin A enhances vascular oxidative stress and the development of angiotensin II-induced aortic aneurysms. *Nat. Med.* 15:649–656. doi:10.1038/nm.1958

Seizer, P., T. Schönberger, M. Schött, M.R. Lang, H.F. Langer, B. Bigalke, B.F. Krämer, O. Borst, K. Daub, O. Heidenreich, et al. 2010. EMMPRIN and its ligand cyclophilin A regulate MT1-MMP, MMP-9 and M-CSF during foam cell formation. *Atherosclerosis.* 209:51–57. doi:10.1016/j.atherosclerosis.2009.08.029

Sherry, B., N. Yarlett, A. Strupp, and A. Cerami. 1992. Identification of cyclophilin as a proinflammatory secretory product of lipopolysaccharide-activated macrophages. *Proc. Natl. Acad. Sci. USA.* 89:3511–3515. doi:10.1073/pnas.89.8.3511

Suzuki, J., Z.G. Jin, D.F. Meoli, T. Matoba, and B.C. Berk. 2006. Cyclophilin A is secreted by a vesicular pathway in vascular smooth muscle cells. *Circ. Res.* 98:811–817. doi:10.1161/01.RES.0000216405.85080.a6

Tangirala, R.K., E.M. Rubin, and W. Palinski. 1995. Quantitation of atherosclerosis in murine models: correlation between lesions in the aortic origin and in the entire aorta, and differences in the extent of lesions between sexes in LDL receptor-deficient and apolipoprotein E-deficient mice. *J. Lipid Res.* 36:2320–2328.

Tegeder, I., A. Schumacher, S. John, H. Geiger, G. Geisslinger, H. Bang, and K. Brune. 1997. Elevated serum cyclophilin levels in patients with severe sepsis. *J. Clin. Immunol.* 17:380–386. doi:10.1023/A:1027364207544

Uittenbogaard, A., Y. Ying, and E.J. Smart. 1998. Characterization of a cytosolic heat-shock protein-caveolin chaperone complex. Involvement in cholesterol trafficking. *J. Biol. Chem.* 273:6525–6532. doi:10.1074/jbc.273.11.6525

Vaziri, N.D., K. Liang, and H. Azad. 2000. Effect of cyclosporine on HMG-CoA reductase, cholesterol 7alpha-hydroxylase, LDL receptor, HDL receptor, VLDL receptor, and lipoprotein lipase expressions. *J. Pharmacol. Exp. Ther.* 294:778–783.

Weber, C., A. Zernecke, and P. Libby. 2008. The multifaceted contributions of leukocyte subsets to atherosclerosis: lessons from mouse models. *Nat. Rev. Immunol.* 8:802–815. doi:10.1038/nri2415

Weintraub, N.L. 2009. Understanding abdominal aortic aneurysm. *N. Engl. J. Med.* 361:1114–1116. doi:10.1056/NEJMcibr0905244

Won, D., S.N. Zhu, M. Chen, A.M. Teichert, J.E. Fish, C.C. Matouk, M. Bonert, M. Ojha, P.A. Marsden, and M.I. Cybulsky. 2007. Relative reduction of endothelial nitric-oxide synthase expression and transcription in atherosclerosis-prone regions of the mouse aorta and in an in vitro model of disturbed flow. *Am. J. Pathol.* 171:1691–1704. doi:10.2353/ajpath.2007.060860

Xu, Q., M.C. Leiva, S.A. Fischkoff, R.E. Handschumacher, and C.R. Lyttle. 1992. Leukocyte chemotactic activity of cyclophilin. *J. Biol. Chem.* 267:11968–11971.

Yurchenko, V., G. Zybarth, M. O'Connor, W.W. Dai, G. Franchin, T. Hao, H. Guo, H.C. Hung, B. Toole, P. Gallay, et al. 2002. Active site residues of cyclophilin A are crucial for its signaling activity via CD147. *J. Biol. Chem.* 277:22959–22965. doi:10.1074/jbc.M201593200

Zhu, C., X. Wang, J. Deinum, Z. Huang, J. Gao, N. Modjtahedi, M.R. Neagu, M. Nilsson, P.S. Eriksson, H. Hagberg, et al. 2007. Cyclophilin A participates in the nuclear translocation of apoptosis-inducing factor in neurons after cerebral hypoxia-ischemia. *J. Exp. Med.* 204:1741–1748. doi:10.1084/jem.20070193

JEM

SUPPLEMENTAL MATERIAL

Nigro et al., http://www.jem.org/cgi/content/full/jem.20101174/DC1

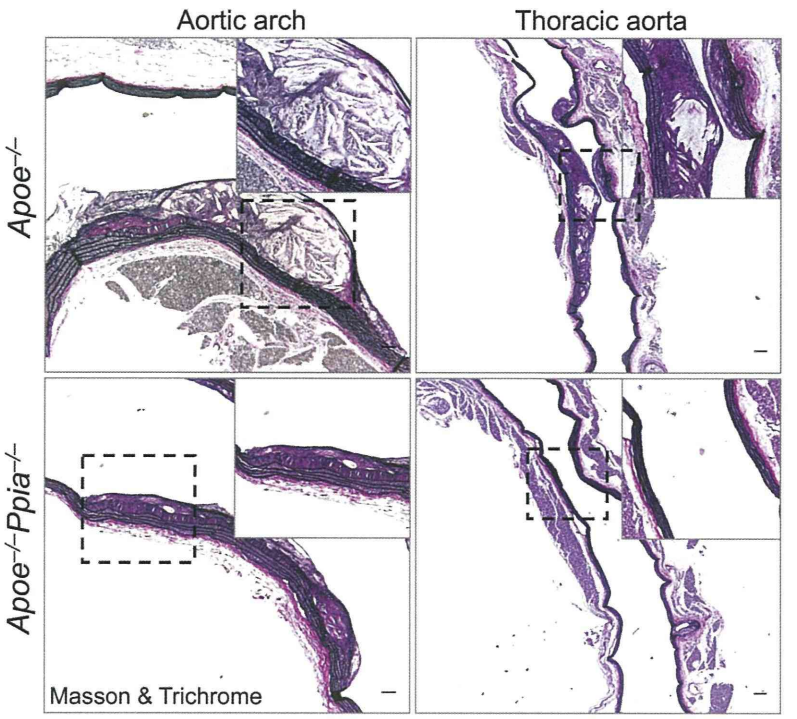

Figure S1. CyPA deficiency prevents atherosclerosis formation. Representative examples of aortic longitudinal cross sections from the aortic arch and thoracic aorta stained with Masson and Trichrome. *Apoe*$^{-/-}$*Ppia*$^{-/-}$ mice are protected in the elastin degradation in both the aortic arch and thoracic aorta. Insets show higher magnification images of areas in the dashed boxes. Data are representative of two separate experiments with similar results (n = 4 each group). Bars: (left) 25 µm; (right) 200 µm.

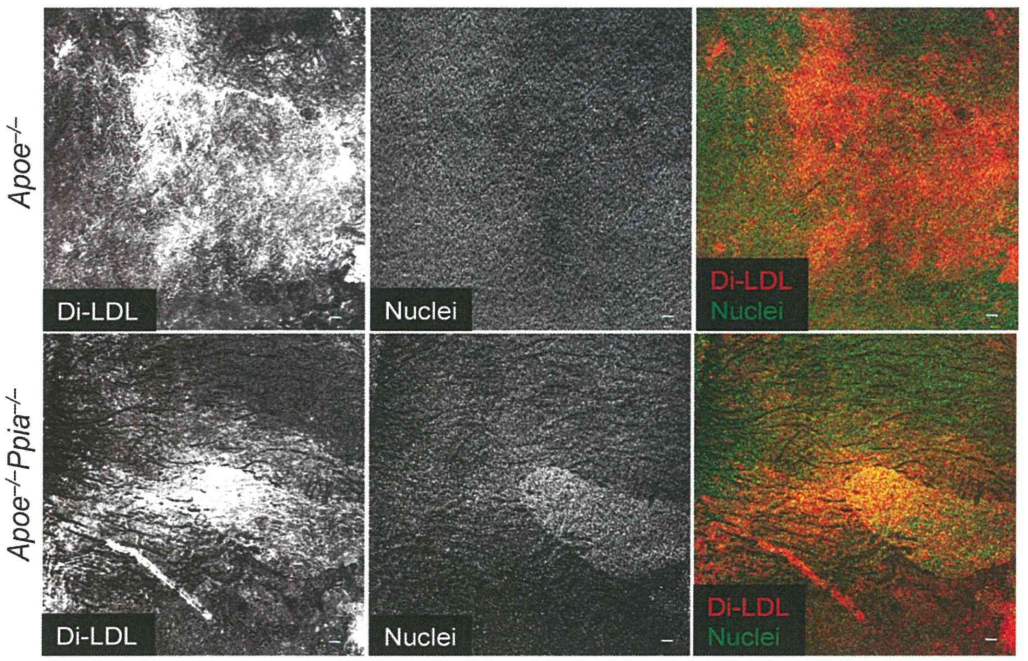

Figure S2. CyPA deficiency decreases LDL uptake in the lesser curvature of the mouse aorta. Aortas from *Apoe*$^{-/-}$ (n = 4) and *Apoe*$^{-/-}$*Ppia*$^{-/-}$ (n = 4) mice were harvested for qualitative analysis of DiI-labeled LDL uptake in the athero-prone areas of the aortic arch. Data are representative of two separate experiments with similar results. Bars, 50 µm.

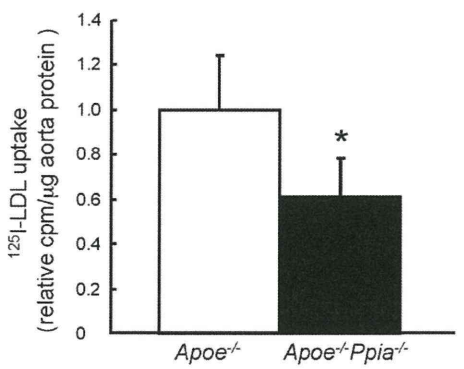

Figure S3. CyPA regulates LDL uptake. Aortas from *Apoe*$^{-/-}$ (n = 4) and *Apoe*$^{-/-}$*Ppia*$^{-/-}$ (n = 4) mice were incubated with [^{125}I]LDL uptake for 3 h. Measurement of cell-associated label was performed in a gamma counter. Results are mean ± SD; *, $P < 0.01$ compared with *Apoe*$^{-/-}$ mice. Results show pooled data from two experiments.

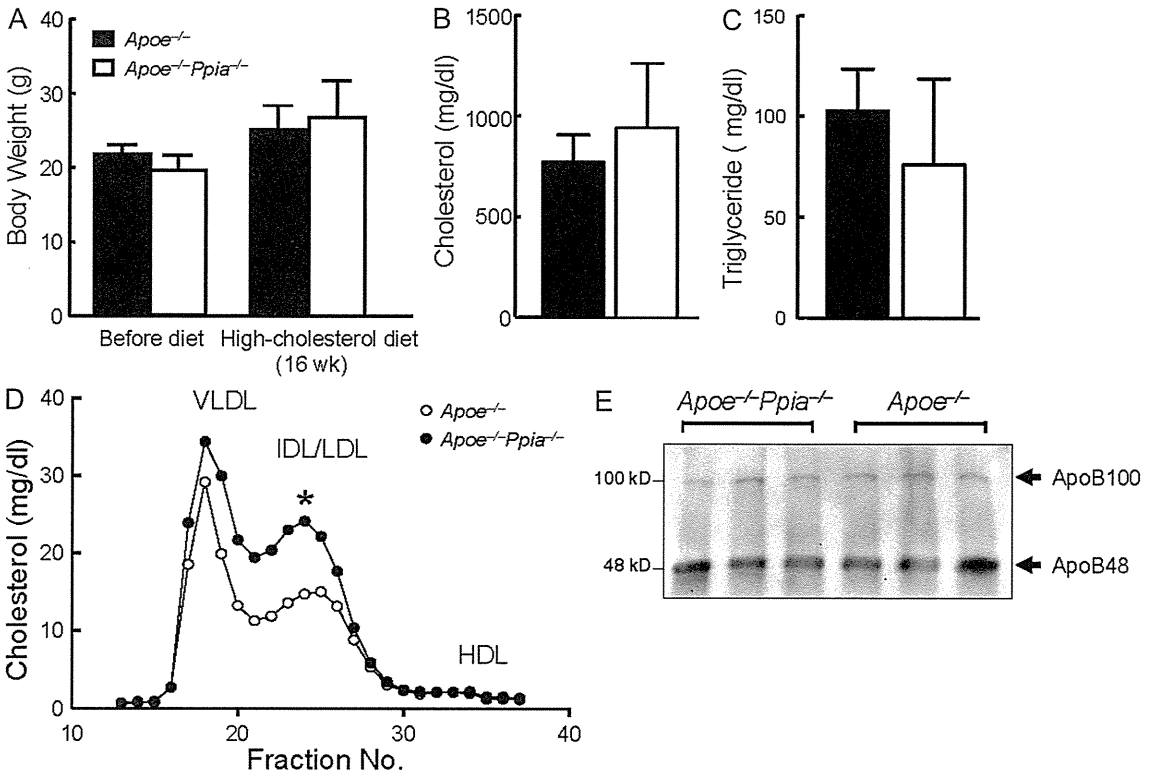

Figure S4. Metabolic parameters in the absence of CyPA. (A) Body weight of *Apoe*$^{-/-}$ (n = 8) and *Apoe*$^{-/-}$*Ppia*$^{-/-}$ (n = 10) mice before and after 16 wk on a high-cholesterol diet. (B and C) Total cholesterol (B) and triglyceride (C) levels of *Apoe*$^{-/-}$ (n = 18) and *Apoe*$^{-/-}$*Ppia*$^{-/-}$ (n = 18) mice after 16 wk on a high-cholesterol diet. (D) Lipoprotein profiles from *Apoe*$^{-/-}$ (n = 9) and *Apoe*$^{-/-}$*Ppia*$^{-/-}$ (n = 9) mice after 16 wk of a high-cholesterol diet. (E) Levels of apoB-100 and apoB-48, the main protein markers of LDL, were determined by Western blot analysis. Plasma apoB levels were similar in animals fed a high-cholesterol diet. Results with three representative animals are shown for each genotype. Equal volumes of plasma were loaded in each lane. Results in A–D are mean ± SD; *, $P < 0.01$ compared with *Apoe*$^{-/-}$ mice. Results in A–D show pooled data from two experiments.

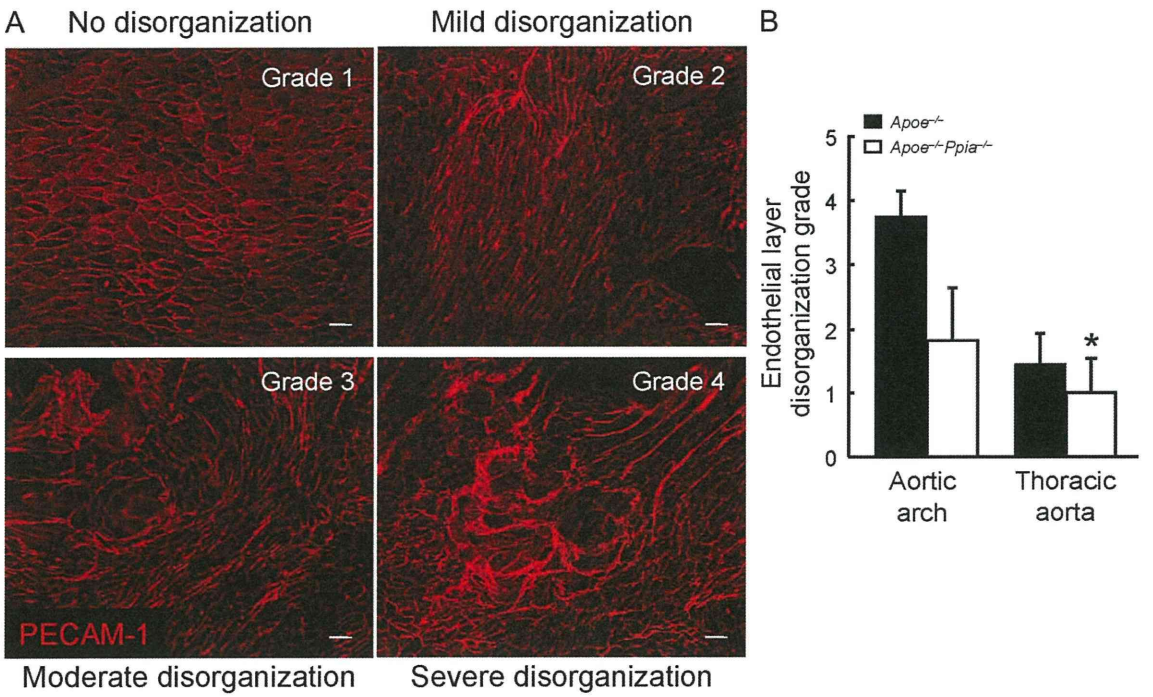

Figure S5. CyPA promotes EC damage and disorganization. (A) EC disorganization-grading (four grades) keys by using PECAM-1 en face aortic staining. Bars, 10 µm. (B) Statistical analysis based on the EC layer disorganization grade shows a significant decrease in EC damage in *Apoe*$^{-/-}$*Ppia*$^{-/-}$ mice compared with *Apoe*$^{-/-}$ mice (n = 4 each group). Results are mean ± SD; *, $P < 0.01$ compared with *Apoe*$^{-/-}$ mice. Results in B show pooled data from two experiments.

Arteriosclerosis, Thrombosis, and Vascular Biology

JOURNAL OF THE AMERICAN HEART ASSOCIATION

Cyclophilin A Promotes Cardiac Hypertrophy in Apolipoprotein E–Deficient Mice

Kimio Satoh, Patrizia Nigro, Asad Zeidan, Nwe Nwe Soe, Fabrice Jaffré, Masayoshi Oikawa, Michael R. O'Dell, Zhaoqiang Cui, Prashanthi Menon, Yan Lu, Amy Mohan, Chen Yan, Burns C. Blaxall and Bradford C. Berk

Arterioscler Thromb Vasc Biol. 2011;31:1116-1123; originally published online February 17, 2011;
doi: 10.1161/ATVBAHA.110.214601
Arteriosclerosis, Thrombosis, and Vascular Biology is published by the American Heart Association, 7272 Greenville Avenue, Dallas, TX 75231

Print ISSN: 1079-5642. Online ISSN: 1524-4636

Cyclophilin A Promotes Cardiac Hypertrophy in Apolipoprotein E–Deficient Mice

Kimio Satoh, Patrizia Nigro, Asad Zeidan, Nwe Nwe Soe, Fabrice Jaffré, Masayoshi Oikawa, Michael R. O'Dell, Zhaoqiang Cui, Prashanthi Menon, Yan Lu, Amy Mohan, Chen Yan, Burns C. Blaxall, Bradford C. Berk

Objective—Cyclophilin A (CyPA, encoded by *Ppia*) is a proinflammatory protein secreted in response to oxidative stress in mice and humans. We recently demonstrated that CyPA increased angiotensin II (Ang II)–induced reactive oxygen species (ROS) production in the aortas of apolipoprotein E ($Apoe^{-/-}$) mice. In this study, we sought to evaluate the role of CyPA in Ang II–induced cardiac hypertrophy.

Methods and Results—Cardiac hypertrophy was not significantly different between $Ppia^{+/+}$ and $Ppia^{-/-}$ mice infused with Ang II (1000 ng/min per kg for 4 weeks). Therefore, we investigated the effect of CyPA under conditions of high ROS and inflammation using the $Apoe^{-/-}$ mice. In contrast to $Apoe^{-/-}$ mice, $Apoe^{-/-}Ppia^{-/-}$ mice exhibited significantly less Ang II–induced cardiac hypertrophy. Bone marrow cell transplantation showed that CyPA in cells intrinsic to the heart plays an important role in the cardiac hypertrophic response. Ang II–induced ROS production, cardiac fibroblast proliferation, and cardiac fibroblast migration were markedly decreased in $Apoe^{-/-}Ppia^{-/-}$ cardiac fibroblasts. Furthermore, CyPA directly induced the hypertrophy of cultured neonatal cardiac myocytes.

Conclusion—CyPA is required for Ang II–mediated cardiac hypertrophy by directly potentiating ROS production, stimulating the proliferation and migration of cardiac fibroblasts, and promoting cardiac myocyte hypertrophy. (***Arterioscler Thromb Vasc Biol.* 2011;31:1116-1123.**)

Key Words: cardiac hypertrophy ■ cardiac remodeling ■ oxidative stress

Cardiac hypertrophy is a fundamental response of cardiac cells to common clinical disorders, such as arterial hypertension, valvular heart disease, myocardial infarction, cardiomyopathy, and congenital heart disease.[1] Emerging data reveal that the communication between cardiac fibroblasts and myocytes plays a critical role in cell-cell signaling in the heart, and it is implicated in the process of cardiac remodeling and overall heart function during development and cardiopathology.[2–5] There are numerous lines of evidence indicating that cardiac fibroblasts and myocytes release into their local microenvironment proteins that regulate neighboring cells via paracrine mechanisms.[2–5] Although multiple factors have been implicated in this intercellular crosstalk, the discovery of new hypertrophic players and a better understanding of the underlying mechanisms hold the key to successful therapy of hypertrophic heart disease.

Cyclophilin A (CyPA, encoded by *Ppia*) was originally found as a binding partner of cyclosporine A.[6] Intracellular CyPA is a chaperone protein that has several functions, including peptidyl-prolyl isomerase activity and protein trafficking, such as nuclear translocation of ERK1/2[7] and apoptosis-inducing factor.[8] We and others have provided evidence that CyPA is secreted in response to reactive oxygen species (ROS) from vascular smooth muscle cells[9] and rat neonatal cardiac myocytes.[10] Moreover, we have shown the involvement of CyPA in angiotensin II (Ang II)–induced aortic aneurysms and oxidative stress.[11,12]

Ang II plays a key role in many physiological and pathological processes in cardiac cells, including cardiac hypertrophy.[13] Therefore, understanding the molecular mechanisms responsible for Ang II–mediated myocardial pathophysiology will be critical to developing new therapies for cardiac dysfunction.[14] One important mechanism now recognized to be involved in Ang II–induced cardiac hypertrophy is ROS production,[15,16] but the precise mechanism by which ROS cause hypertrophy remains unknown. Our recent study provides strong mechanistic evidence of synergy between CyPA and Ang II to increase ROS generation.[11]

Received on: August 13, 2010; final version accepted on: January 27, 2011.

From the Aab Cardiovascular Research Institute (K.S., P.N., A.Z., N.N.S., F.J., M.O., M.R.O., Z.C., P.M., Y.L., A.M., C.Y., B.C. Blaxall, B.C. Berk) and Department of Medicine (K.S., P.N., A.Z., N.N.S., F.J., M.O., M.R.O., Z.C., P.M., Y.L., A.M., C.Y., B.C. Blaxall, B.C. Berk), University of Rochester School of Medicine and Dentistry, Rochester, NY; Department of Cardiovascular Medicine, Tohoku University Graduate School of Medicine, Aoba-ku, Sendai, Japan (K.S.).

Drs Satoh and Nigro contributed equally to this work.

Correspondence to Bradford C. Berk, MD, PhD, Aab Cardiovascular Research Institute, University of Rochester, Box CVRI, 601 Elmwood Ave, Rochester, NY 14642. E-mail bradford_berk@urmc.rochester.edu

Arterioscler Thromb Vasc Biol **is available at http://atvb.ahajournals.org** **DOI: 10.1161/ATVBAHA.110.214601**

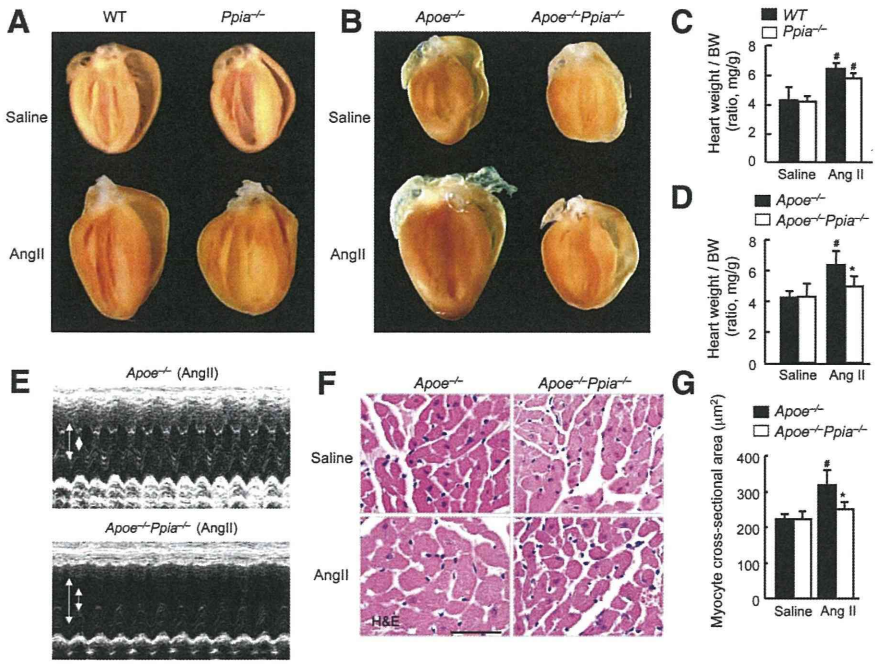

Figure 1. CyPA deficiency prevents Ang II–induced cardiac hypertrophy in *Apoe*$^{-/-}$ mice. A, Representative photographs showing macroscopic features of cardiac hypertrophy induced by Ang II infusion in *Ppia*$^{-/-}$ mice vs WT mice. Ang II–induced cardiac hypertrophy was not prevented in *Ppia*$^{-/-}$ mice compared with WT mice. B, Representative photographs of the hearts of *Apoe*$^{-/-}$ and *Apoe*$^{-/-}$*Ppia*$^{-/-}$ mice infused with Ang II or saline for 4 weeks. Ang II–induced cardiac hypertrophy was prevented in *Apoe*$^{-/-}$*Ppia*$^{-/-}$ mice compared with *Apoe*$^{-/-}$ mice. C, Ang II–induced cardiac hypertrophy (heart weight/BW ratio) was not significantly decreased in *Ppia*$^{-/-}$ mice (n=5) compared with WT (n=6). #P<0.05 in saline vs Ang II; *P<0.05 in *WT* vs *Ppia*$^{-/-}$ mice. D, Ang II–induced cardiac hypertrophy (heart weight/BW ratio) was significantly reduced in *Apoe*$^{-/-}$*Ppia*$^{-/-}$ mice (n=11) compared with *Apoe*$^{-/-}$ mice (n=15). No significant differences were found in the control groups (saline infusion) of *Apoe*$^{-/-}$ and *Apoe*$^{-/-}$*Ppia*$^{-/-}$ mice (n=4, respectively). E, Representative M-mode images of cardiac hypertrophy assessed by echocardiography after 4 weeks of Ang II infusion. Arrows indicate the diastolic LV cavity and systolic LV cavity. F, H&E staining of representative cross-sections of cardiac myocytes of *Apoe*$^{-/-}$ and *Apoe*$^{-/-}$*Ppia*$^{-/-}$ mice 4 weeks after Ang II infusion. G, Myocyte cross-sectional area was significantly reduced in *Apoe*$^{-/-}$*Ppia*$^{-/-}$ mice (n=7) compared with *Apoe*$^{-/-}$ mice (n=9). Results are mean±SD. #P<0.05 in saline vs Ang II; *P<0.05 in *Apoe*$^{-/-}$ vs *Apoe*$^{-/-}$*Ppia*$^{-/-}$ mice.

Because ROS stimulate myocardial hypertrophy, matrix remodeling, and cellular dysfunction,[17] we tested the hypothesis that CyPA enhances Ang II–induced cardiac ROS production and therefore cardiac hypertrophy.

Methods

An expanded Supplemental Methods section is available online at http://atvb.ahajournals.org.

Analysis of Cardiac Hypertrophy

Ang II–infused models were used to assess the effect of CyPA deficiency on cardiac hypertrophy.[18] Five- to 6-week-old male mice on a normal chow diet were infused with 1000 ng/min per kg Ang II (MP Biomedicals, Solon, OH) or saline vehicle for 4 weeks. Ang II was dissolved in sterile saline and infused using Alzet osmotic pumps (model 2004, Durect Corp, Cupertino, CA). Mice were anesthetized with an intraperitoneal injection of ketamine (80 mg/kg) and xylazine (5 mg/kg). Pumps were placed into the subcutaneous space of anesthetized mice through a small incision in the back of the neck that was closed with suture. After 4 weeks of Ang II infusion, the animals were again anesthetized with ketamine (80 mg/kg) and xylazine (5 mg/kg). The heart tissue was perfused with calcium- and magnesium-free phosphate-buffered saline (PBS) and then fixed with phosphate-buffered 10% formalin solution and subsequently prepared for histological analysis as previously described.[19] Heart weight was measured, and the ratio of heart weight to body weight (BW) was calculated to determine an index of cardiac hypertrophy. Five sections were obtained from each heart and mounted on slides and stained with Masson's trichrome or hematoxylin/eosin (H&E). To evaluate the perivascular fibrosis, short-axis images of coronary arteries were scanned at ×200 magnification. The area of perivascular fibrosis (the ratio of the fibrosis area surrounding the vessel to the total vessel area) was calculated. To evaluate the extent of cardiac myocyte hypertrophy, cross-sectional images of cardiac myocytes were scanned at ×400 magnification. Approximately 10 cross-sections of cardiac myocytes were analyzed in each heart. Average values for each heart were used for analysis.

Bone Marrow Transplantation

Bone marrow transplantation was performed as described.[20] Briefly, recipient mice were lethally irradiated and received an intravenous injection of 5×10^6 donor bone marrow cells suspended in 100 μL of PBS with 2% fetal bovine serum. After transplantation, the mice were placed on a regular chow diet for 6 weeks followed by infusion of 1000 ng/kg per minute Ang II for 4 weeks. Transgenic mice ubiquitously expressing green fluorescent protein (GFP) were obtained from the Jackson Laboratory (Bar Harbor, ME). The chimeric rate assessed by GFP$^+$ cells in the peripheral blood was more than 99% by fluorescence-activated cell sorter analysis (FACSCantoII, Becton Dickinson, San Jose, CA).

ROS Analysis

The evaluation of ROS production in response to Ang II was performed as described before.[21] After treatment with Ang II (1 μmol/L), cardiac fibroblasts were washed with PBS and loaded with 2,7-dichlorofluoresceine diacetate (5 μmol/L; Molecular Probes) for 30 minutes. Hearts were perfused with PBS (pH 7.4) at 100 mm Hg for 5 minutes at 4°C. Heart tissue was harvested and embedded in OCT (Tissue-Tek, Miles Inc., Elkhart, IL) and snap-frozen. Dihydroethidine hydrochloride (5 μmol/L, Molecular Probes) was topically applied to the freshly cut frozen heart sections (10 μm) for 30 minutes at 37°C. Dichlorofluorescein (DCF) and dihydroethidium fluorescence was revealed by confocal microscopy (Olympus, Fluoview).[22]

A lucigenin assay was performed as previously described, with some modifications.[23] Briefly, control cells or cells treated with Ang II for 4 hours were harvested and pelleted by centrifugation (1200 rpm, 4°C, 5 minutes). To start the assay, cells were resuspended in Hanks' balanced salt solution (Cellegro) containing lucigenin (final concentration, 500 μmol/L). Photon emission was measured every 15 seconds for 20 minutes in a luminometer (Wallac Plate Reader, model 1420). A buffer blank (<5% of the cell signal) was subtracted from each reading before transformation of the data.

[^{3}H]Leucine Incorporation Study

The effect of conditioned medium (CM) from Ang II–stimulated cardiac fibroblasts for protein synthesis in cardiac myocytes was

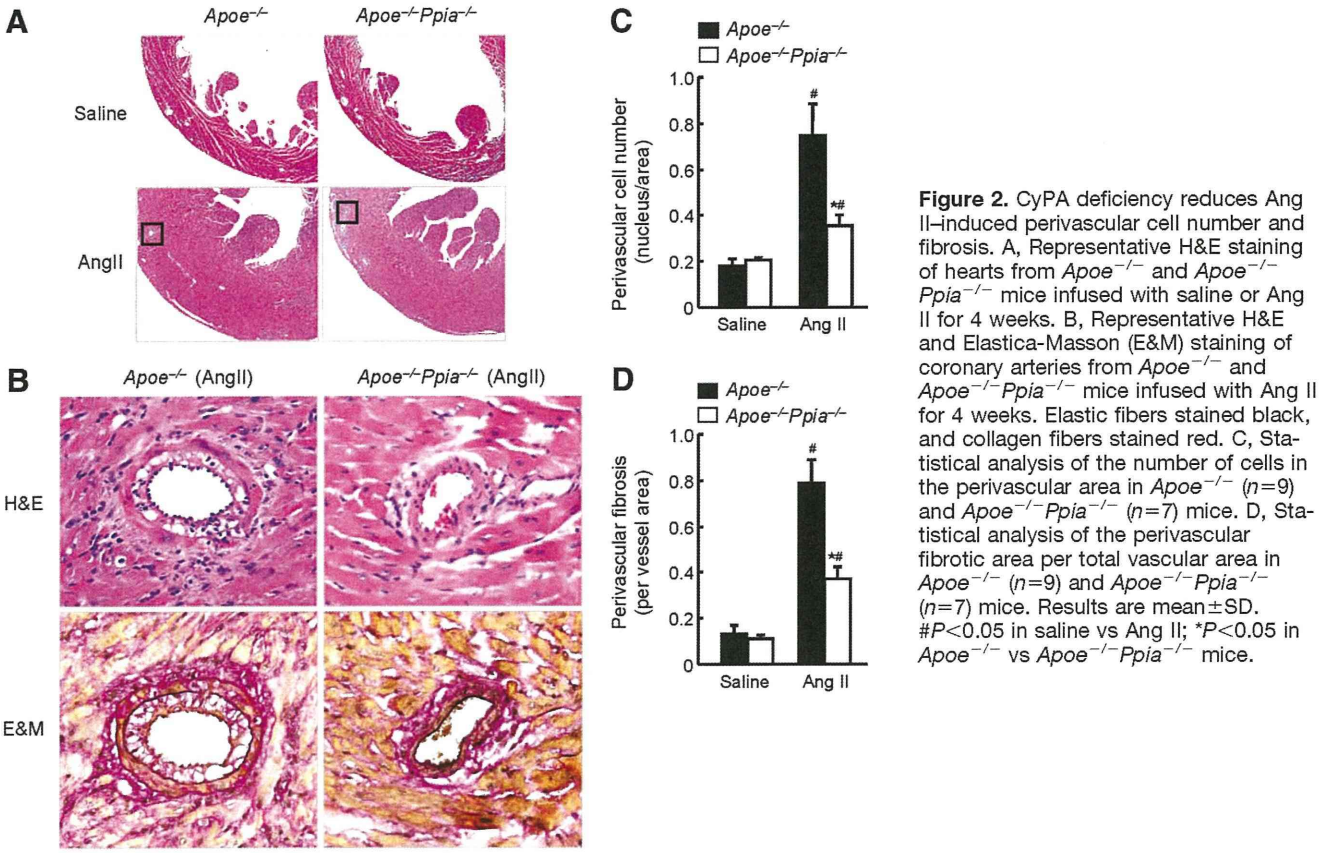

Figure 2. CyPA deficiency reduces Ang II–induced perivascular cell number and fibrosis. A, Representative H&E staining of hearts from *Apoe*$^{-/-}$ and *Apoe*$^{-/-}$ *Ppia*$^{-/-}$ mice infused with saline or Ang II for 4 weeks. B, Representative H&E and Elastica-Masson (E&M) staining of coronary arteries from *Apoe*$^{-/-}$ and *Apoe*$^{-/-}$*Ppia*$^{-/-}$ mice infused with Ang II for 4 weeks. Elastic fibers stained black, and collagen fibers stained red. C, Statistical analysis of the number of cells in the perivascular area in *Apoe*$^{-/-}$ (n=9) and *Apoe*$^{-/-}$*Ppia*$^{-/-}$ (n=7) mice. D, Statistical analysis of the perivascular fibrotic area per total vascular area in *Apoe*$^{-/-}$ (n=9) and *Apoe*$^{-/-}$*Ppia*$^{-/-}$ (n=7) mice. Results are mean±SD. #P<0.05 in saline vs Ang II; *P<0.05 in *Apoe*$^{-/-}$ vs *Apoe*$^{-/-}$*Ppia*$^{-/-}$ mice.

determined by [^{3}H]leucine incorporation as previously described.[24] Briefly, neonatal rat cardiac myocytes were plated at a density of 250,000 cells/well in 12-well plates and maintained in Dulbecco's modified Eagle's medium supplemented with insulin, transferrin, and selenium, 5% horse serum, 5% fetal calf serum, 50 U/mL penicillin, and 50 μg/mL streptomycin for 24 hours. The cells were then starved in serum-free Dulbecco's modified Eagle's medium for 48 hours. Cardiac myocytes were stimulated with cardiac fibroblast-derived CM for 24 hours following incubation with [^{3}H]leucine (2 μCi/mL) for 24 hours. To precipitate proteins, ice-cold 10% trichloroacetic acid was added to the wells. After 30 minutes of incubation on ice, the myocytes were lysed with 0.5 N NaOH and incubated for 10 minutes on ice. All samples were mixed with scintillation cocktail (Biosafe-II) before counting.

Statistical Analysis

Quantitative results are expressed as mean±SD. Comparisons of parameters among 2 groups were made by the unpaired Student t test. Comparisons of parameters among >2 groups were made by 1-way ANOVA, and comparisons of different parameters between the 2 genotypes were made by 2-way analysis of variance (ANOVA), followed by a post hoc analysis using the Bonferroni test. Statistical significance was evaluated with StatView (StatView 5.0, SAS Institute Inc, Cary, NC). A value of P<0.05 was considered to be statistically significant.

Results

CyPA Augments Ang II–Induced Cardiac Hypertrophy In Vivo

To define the role of CyPA in cardiac hypertrophy, we studied the *Ppia*$^{-/-}$ (knockout) and wild-type (WT) mice following Ang II infusion for 4 weeks. Ang II significantly increased heart weight/BW in both *Ppia*$^{-/-}$ and WT mice (Figure 1A and 1C). However, there were no significant differences in heart weight/BW (Figure 1A and 1C), systolic blood pressure, or interventricular septum thickness (Supplemental Table I) between *Ppia*$^{-/-}$ and WT mice before or after Ang II treatment. Although there was an apparent increase in echo-estimated left ventricle (LV) mass in the WT compared with *Ppia*$^{-/-}$, when gravimetric heart was normalized to the BW, the relative increase in heart weight/BW did not differ significantly (1.25-fold versus 1.20-fold).

Because CyPA is a proinflammatory cytokine secreted in response to oxidative stress, we hypothesized that the role of CyPA in cardiac hypertrophy would require a situation in which there was increased ROS generation or inflammation. Previously, it was demonstrated that the hearts of apolipoprotein E (*Apoe*)$^{-/-}$ mice exhibit increased ROS production.[11] Because we showed that ROS generation stimulates secretion of CyPA from vascular smooth muscle cells, we compared the secretion of CyPA from WT and *Apoe*$^{-/-}$ cardiac fibroblasts in response to Ang II. Secretion of CyPA was barely detected in conditioned media (CM) from WT fibroblasts (Supplemental Figure I). In contrast, there was abundant CyPA secretion from Ang II–treated *Apoe*$^{-/-}$ cardiac fibroblasts. We attempted similar experiments in cultured adult cardiac myocytes. However, substantial cell death ensued on culture in the required serum-free medium.

The above data suggest that *Apoe*$^{-/-}$ mice would provide an ideal model by which to study the role of CyPA in Ang II–induced cardiac hypertrophy. Consistent with previous findings,[18] we showed that Ang II infusion for 4 weeks significantly increased cardiac hypertrophy in *Apoe*$^{-/-}$ mice (Figure 1B and 1D). Despite equal increases in blood pressure (Supplemental

Figure IIA), *Apoe*$^{-/-}$*Ppia*$^{-/-}$ mice had significantly smaller increases in heart weight after treatment with Ang II compared with *Apoe*$^{-/-}$ mice (Figure 1B and 1D). Echocardiography showed no significant difference in LV mass and interventricular septum thickness between *Apoe*$^{-/-}$ and *Apoe*$^{-/-}$*Ppia*$^{-/-}$ mice before Ang II treatment (Supplemental Table II). However, after Ang II infusion, *Apoe*$^{-/-}$*Ppia*$^{-/-}$ mice had significantly smaller increases in LV mass and interventricular septum thickness compared with *Apoe*$^{-/-}$ mice (Figure 1E, Supplemental Figure IIB and IIC). Moreover, in *Apoe*$^{-/-}$ mice, Ang II significantly increased cardiac myocyte size compared with control (saline-infused mice) (Figure 1F and 1G). In contrast, in *Apoe*$^{-/-}$*Ppia*$^{-/-}$ mice, Ang II–induced cardiac myocyte hypertrophy was significantly reduced (Figure 1F and 1G). These results suggest that CyPA is required for cardiac hypertrophy induced by Ang II in *Apoe*$^{-/-}$ mice.

Morphologically, the hearts of saline-infused *Apoe*$^{-/-}$*Ppia*$^{-/-}$ mice did not differ from the hearts of *Apoe*$^{-/-}$ mice, as shown by H&E staining (Figure 2A). In response to Ang II, LV wall thickness significantly increased in *Apoe*$^{-/-}$ and *Apoe*$^{-/-}$*Ppia*$^{-/-}$ mice, although to a lesser extent in *Apoe*$^{-/-}$*Ppia*$^{-/-}$ mice (Figure 2A). Most impressively, there was an obvious reduction in perivascular cell number, suggesting decreased proliferation or migration of cells to the perivascular area in the *Apoe*$^{-/-}$*Ppia*$^{-/-}$ mice (Figure 2B and 2C). There was also a decrease in collagen content in the perivascular area, as shown by Elastica-Masson staining (Figure 2B), in the *Apoe*$^{-/-}$*Ppia*$^{-/-}$ mice after Ang II treatment. Perivascular fibrosis area was markedly decreased in the coronary arteries of *Apoe*$^{-/-}$*Ppia*$^{-/-}$ mice (Figure 2D). These data suggest that CyPA contributes to cardiac hypertrophy and perivascular fibrosis in *Apoe*$^{-/-}$ mice.

CyPA Deficiency Prevents Ang II–Induced ROS Production in Cardiac Tissue

Because ROS are key mediators of Ang II action, we next investigated whether CyPA altered the redox state of the heart after Ang II treatment. Heart sections were incubated with dihydroethidium, which in the presence of superoxide anions is transformed to fluorescent oxyethidium. In the saline-infused heart, ROS production (red fluorescence) was low in both *Apoe*$^{-/-}$ and *Apoe*$^{-/-}$*Ppia*$^{-/-}$ mice (Figure 3A, 3B, and 3E). After Ang II treatment, in the whole heart, oxyethidium fluorescence was ≈2-fold greater in *Apoe*$^{-/-}$ mice compared with *Apoe*$^{-/-}$*Ppia*$^{-/-}$ mice (Figure 3C, 3D, and 3E). In the perivascular area of *Apoe*$^{-/-}$ mice, ROS production was increased by 4-fold after Ang II–treatment (Figure 3C and 3F). In contrast, in *Apoe*$^{-/-}$*Ppia*$^{-/-}$ mice, the perivascular increase in ROS was markedly reduced (Figure 3D and 3F). These data suggest that CyPA is a key determinant for Ang II–mediated ROS production.

Cardiac-Derived CyPA Promotes Recruitment of Bone Marrow–Derived Cells

We have shown that CyPA has direct chemotactic effects on bone marrow–derived cells and promotes vascular cell proliferation and remodeling.[19] To determine whether cardiac CyPA promotes recruitment of bone marrow–derived cells and mediates Ang II–induced cardiac hypertrophy, GFP$^+$

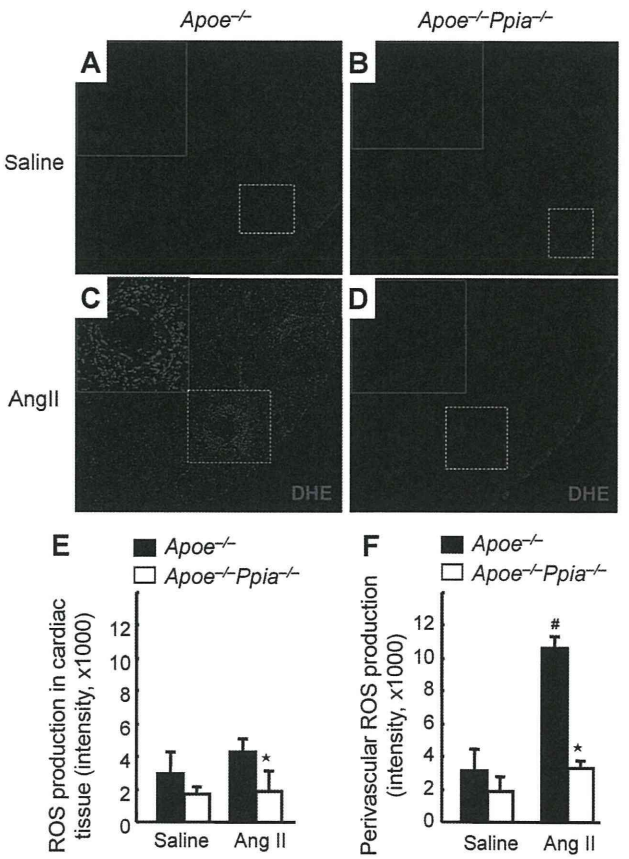

Figure 3. CyPA is crucial for cardiac ROS formation. A to D, Representative in situ dihydroethidium (DHE) staining of hearts. The hearts from *Apoe*$^{-/-}$ and *Apoe*$^{-/-}$*Ppia*$^{-/-}$ mice infused with saline or Ang II for 7 days were used for analysis. Images were obtained using the same magnification (×100) and shutter speed. E and F, Densitometric analysis of oxyethidium (red fluorescence) in the cardiac tissue (E) and the perivascular area (F). Results are mean±SD (n=4 in each group). #P<0.05 in saline vs Ang II; *P<0.05 in *Apoe*$^{-/-}$ vs *Apoe*$^{-/-}$*Ppia*$^{-/-}$ mice.

bone marrow cells (*Ppia*$^{+/+}$) were transplanted into irradiated *Apoe*$^{-/-}$ or *Apoe*$^{-/-}$*Ppia*$^{-/-}$ mice. After 42 days, these chimeric mice were treated with Ang II for 4 weeks. There was no significant difference in the blood pressure between chimeric mice before and after Ang II infusion (data not shown). Ang II dramatically increased the number of bone marrow–derived cells (GFP$^+$ cells) present in the cardiac tissue in the *Apoe*$^{-/-}$ recipient mice (Figure 4C and 4E). Most significant was the accumulation of bone marrow–derived cells in the perivascular area of *Apoe*$^{-/-}$ recipient mice (Figure 4C and 4F), which was significantly reduced in the perivascular area of *Apoe*$^{-/-}$*Ppia*$^{-/-}$ recipient mice (Figure 4D and 4F). Because many of these bone marrow–derived cells are inflammatory cells, and inflammation is associated with increased ROS, it is possible that they will contribute to the elevated ROS observed in the perivascular area.

After transplantation of *Ppia*$^{+/+}$ bone marrow cells to the *Apoe*$^{-/-}$*Ppia*$^{-/-}$ mice, cardiac hypertrophy was still significantly lower in *Apoe*$^{-/-}$*Ppia*$^{-/-}$ recipient mice compared with *Apoe*$^{-/-}$ recipient mice (Figure 4G). These data suggest that *Ppia*$^{+/+}$ inflammatory cells are not important in Ang II–induced cardiac hypertrophy. We next prepared chimeric

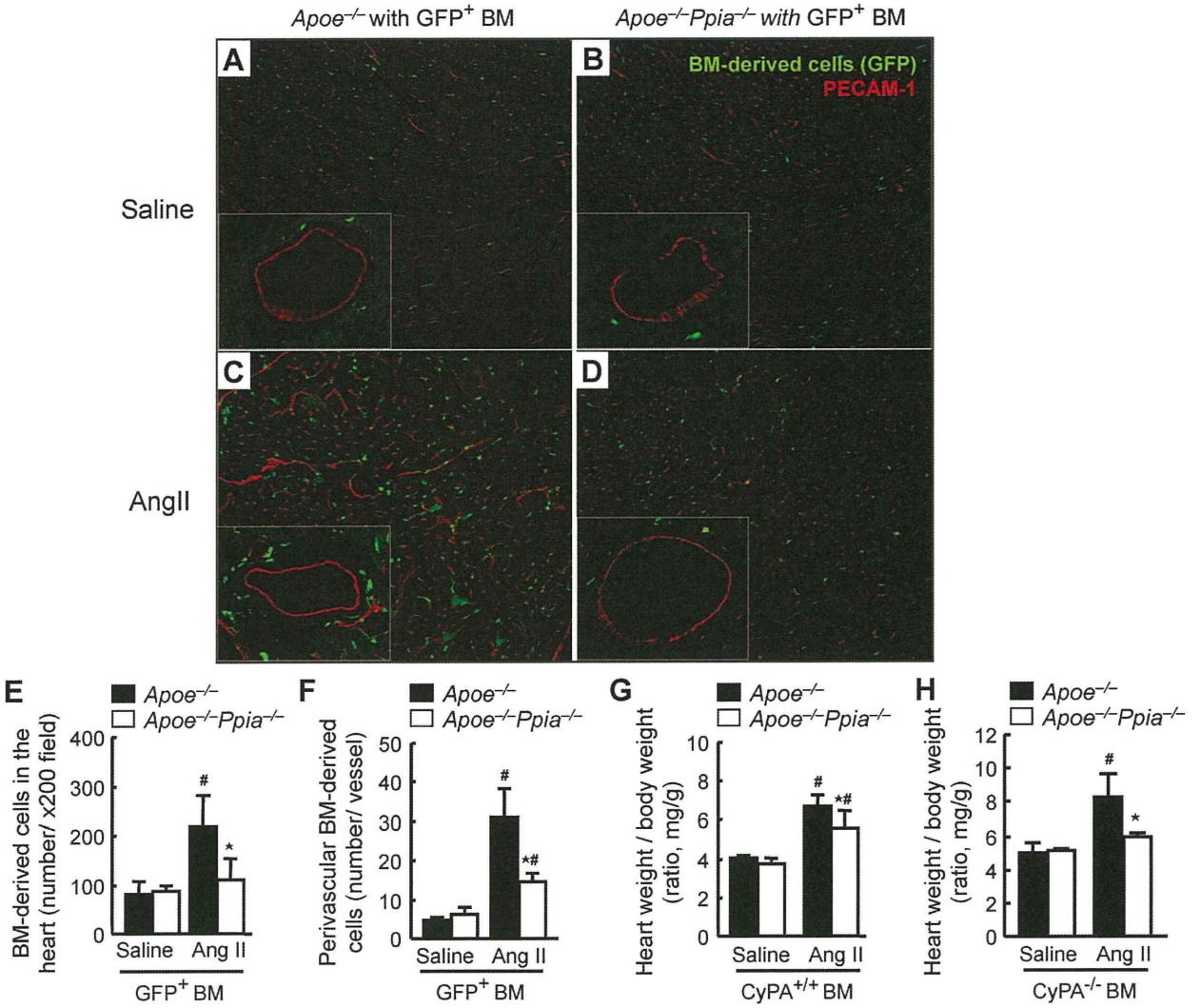

Figure 4. Bone marrow reconstitution shows a strong effect of cardiac CyPA for recruitment of bone marrow–derived cells in response to Ang II and development of cardiac hypertrophy. GFP$^+$ bone marrow cells (*Ppia*$^{+/+}$) were transplanted into irradiated *Apoe*$^{-/-}$ or *Apoe*$^{-/-}$*Ppia*$^{-/-}$ mice. After 6 weeks, these chimeric mice with GFP$^+$ bone marrow were infused with saline (A and B) or Ang II for 4 weeks (C and D). A to D, Representative platelet and endothelial cell adhesion molecule-1 staining (red) of hearts from *Apoe*$^{-/-}$ and *Apoe*$^{-/-}$*Ppia*$^{-/-}$ recipient mice with GFP$^+$ bone marrow (green). E and F, Statistical analysis of the number of migrating GFP$^+$ bone marrow cells in the cardiac tissue (E) or perivascular area (F) in the hearts of *Apoe*$^{-/-}$ (n=9) and *Apoe*$^{-/-}$*Ppia*$^{-/-}$ (n=8) mice. G, Ang II–induced cardiac hypertrophy (heart weight/BW ratio) was significantly lower in *Apoe*$^{-/-}$*Ppia*$^{-/-}$ recipient mice (n=9) compared with *Apoe*$^{-/-}$ recipient mice (n=8) with *Ppia*$^{+/+}$ bone marrow. H, Heart weight/BW ratio after Ang II infusion for 4 weeks was significantly lower in *ApoE*$^{-/-}$*Ppia*$^{-/-}$ (n=6) compared with *ApoE*$^{-/-}$ (n=6) chimeric mice with *Ppia*$^{-/-}$ bone marrow. Results are mean±SD. #P<0.05 in saline vs Ang II; *P<0.05 in *Apoe*$^{-/-}$ vs *Apoe*$^{-/-}$*Ppia*$^{-/-}$ mice.

mice transplanted with *Ppia*$^{-/-}$ bone marrow to investigate the role of recipient environment. There was no significant difference in the heart weight/BW of saline-infused groups. However, after Ang II infusion for 4 weeks, there was still a significantly greater heart weight/BW in the *ApoE*$^{-/-}$ compared with the *ApoE*$^{-/-}$*Ppia*$^{-/-}$ chimeric mice, even after transplantation with *Ppia*$^{-/-}$ bone marrow (Figure 4H). These data further demonstrate that cardiac-derived CyPA, not bone marrow–derived CyPA, is most important in Ang II–induced cardiac hypertrophy.

CyPA Augments Ang II–Induced ROS Production and Proliferation in Cultured Cardiac Fibroblasts

On the basis of the above results, we next evaluated the effects of CyPA on cells present in cardiac tissue. We first studied cardiac fibroblasts because of the increase in perivascular collagen (Figure 2B) and the large increase in CyPA secretion (Supplemental Figure I) in response to Ang II. We isolated cardiac fibroblasts from *Apoe*$^{-/-}$ and *Apoe*$^{-/-}$*Ppia*$^{-/-}$ mice and measured ROS by DCF staining. In response to 1 μmol/L Ang II, there was a 2-fold increase in ROS production in *Apoe*$^{-/-}$ (Figure 5A and 5B). There was a dramatic reduction in Ang II–induced ROS production in *Apoe*$^{-/-}$*Ppia*$^{-/-}$ fibroblasts (Figure 5A and 5B), suggesting that CyPA plays an autocrine role in cardiac fibroblast ROS generation, similar to our findings in vascular smooth muscle cells.[11] To verify the results with DCF, we also measured ROS by lucigenin chemiluminescence. As shown in Figure 5C, Ang II–induced ROS production was significantly decreased by ≈50% in *Apoe*$^{-/-}$*Ppia*$^{-/-}$ fibro-

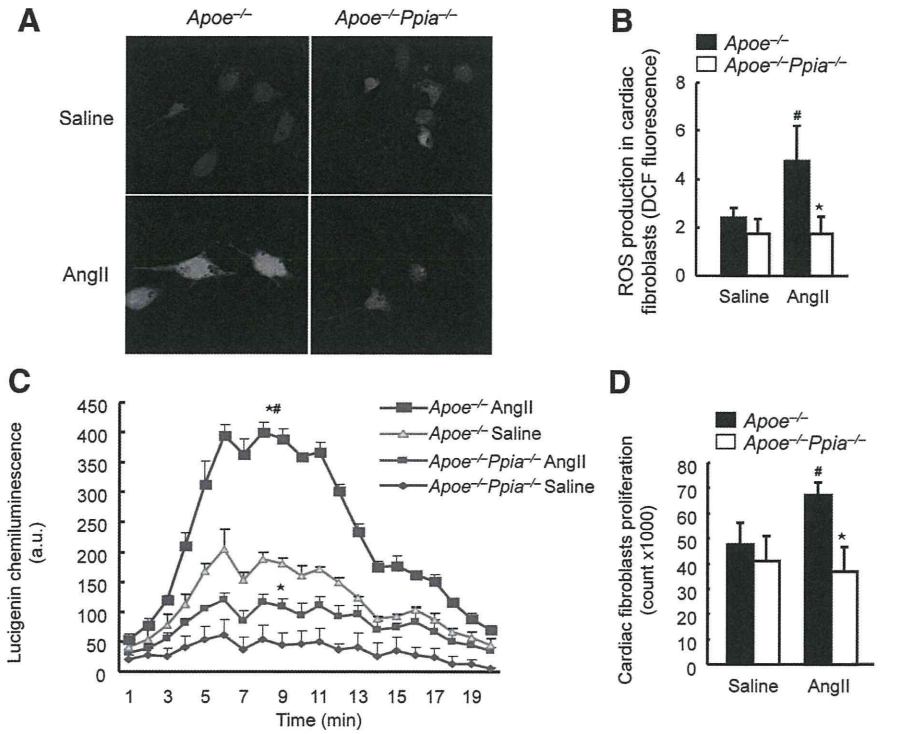

Figure 5. CyPA activates cardiac fibroblasts by enhancing ROS production. A, Representative DCF staining of mouse cardiac fibroblasts. Ang II–induced ROS generation after 4 hours was decreased in CyPA-deficient cardiac fibroblasts. B, Densitometric analysis of DCF fluorescence in response to Ang II shows significant reduction in $Ppia^{-/-}$ cardiac fibroblasts at 4 hours (n=8 in each group). C, Superoxide production in cardiac fibroblasts exposed to lucigenin for 4 hours. Results are mean±SD of 3 independent experiments performed in triplicate. #P<0.05 in saline vs Ang II; *P<0.05 in $Apoe^{-/-}$ vs $Apoe^{-/-}Ppia^{-/-}$ mice. D, Proliferation of cardiac fibroblasts. $Apoe^{-/-}$ and $Apoe^{-/-}Ppia^{-/-}$ fibroblasts were treated with saline or Ang II. After 48 hours of incubation, cells were counted (n=3 in each group). Results are mean±SD. #P<0.05 in saline vs Ang II; *P<0.05 in $Apoe^{-/-}$ vs $Apoe^{-/-}Ppia^{-/-}$ cardiac fibroblasts.

blasts compared with $Apoe^{-/-}$ fibroblasts, similar to results with DCF.

Excessive fibroblast proliferation induces myocardial stiffening, an important component of pathological cardiac hypertrophy.[25,26] To evaluate whether CyPA is important in fibroblast proliferation, cell number in response to Ang II was assessed. Proliferation was significantly augmented by Ang II in $Apoe^{-/-}$ cardiac fibroblasts, whereas there was no change in $Apoe^{-/-}Ppia^{-/-}$ fibroblasts (Figure 5D). These results suggest that CyPA-mediated cardiac fibroblast proliferation contributes to the perivascular cellular response.

Extracellular CyPA Promotes Proliferation and Migration of Cultured Cardiac Fibroblasts

We next evaluated the effect of extracellular CyPA on fibroblast proliferation. Interestingly, there was a small but significantly greater growth rate of $Apoe^{-/-}$ fibroblasts compared with $Apoe^{-/-}Ppia^{-/-}$ fibroblasts treated with vehicle measured by cell number (Figure 6A). Addition of recombinant CyPA (100 nmol/L) significantly increased proliferation of $Apoe^{-/-}$ fibroblasts (Figure 6A) and compared to $Apoe^{-/-}Ppia^{-/-}$ cardiac fibroblasts (Figure 6A).

We next studied the effect of CyPA on migration of fibroblasts. There was a concentration-dependent increase in migration, which was significant at 100 nmol/L CyPA (Figure 6B). These findings highlight the importance of extracellular and intracellular CyPA in cardiac fibroblast proliferation and migration.

Extracellular CyPA Has a Direct Effect on Cardiac Myocyte Hypertrophy

To evaluate whether CyPA could be a direct hypertrophic factor, we investigated the effect of extracellular CyPA on protein synthesis of isolated rat neonatal cardiac myocytes. Treatment with recombinant CyPA significantly increased [^{3}H]leucine incorporation in cardiac myocytes, suggesting the critical role of extracellular CyPA for the hypertrophic response (Figure 6C). To confirm further our data, we measured atrial natriuretic peptide and brain natriuretic peptide mRNA expression, 2 accepted markers of cardiac hypertrophy. We found that CyPA upregulated atrial natriuretic peptide and brain natriuretic peptide in neonatal cardiac myocytes (Figure 6D).

Cardiac fibroblasts isolated from $Apoe^{-/-}$ mice secreted substantial amounts of CyPA in response to Ang II (Supplemental Figure I). Therefore, we investigated the role of fibroblast-derived secreted CyPA in mediating Ang II–induced hypertrophic response in cardiac myocytes. We treated rat neonatal cardiac myocytes with CM prepared from Ang II–stimulated cardiac fibroblasts. Protein synthesis, as measured by [^{3}H]leucine incorporation in myocytes, was used as a parameter of hypertrophy. CM prepared from Ang II–stimulated $Apoe^{-/-}$ fibroblasts significantly augmented [^{3}H]leucine incorporation in cardiac myocytes (Figure 6E). In contrast, there was no effect when myocytes were stimulated with CM prepared from the $Apoe^{-/-}Ppia^{-/-}$ fibroblasts (Figure 6E). These results suggest that CyPA secreted from cardiac fibroblasts can act as a hypertrophic factor on cardiac myocytes. However, on the basis of these data, we cannot exclude the possibility that CyPA is involved in the secretion of another factor, either from fibroblasts or myocytes, which in turn induces cardiac hypertrophy. Together, these results indicate that both intracellular CyPA and extracellular CyPA play critical roles in the mechanisms that contribute to cardiac hypertrophy.

Discussion

The major finding of the present study is that CyPA is a novel mediator of cardiac hypertrophy. We characterized 4 important pathological mechanisms by which CyPA promotes

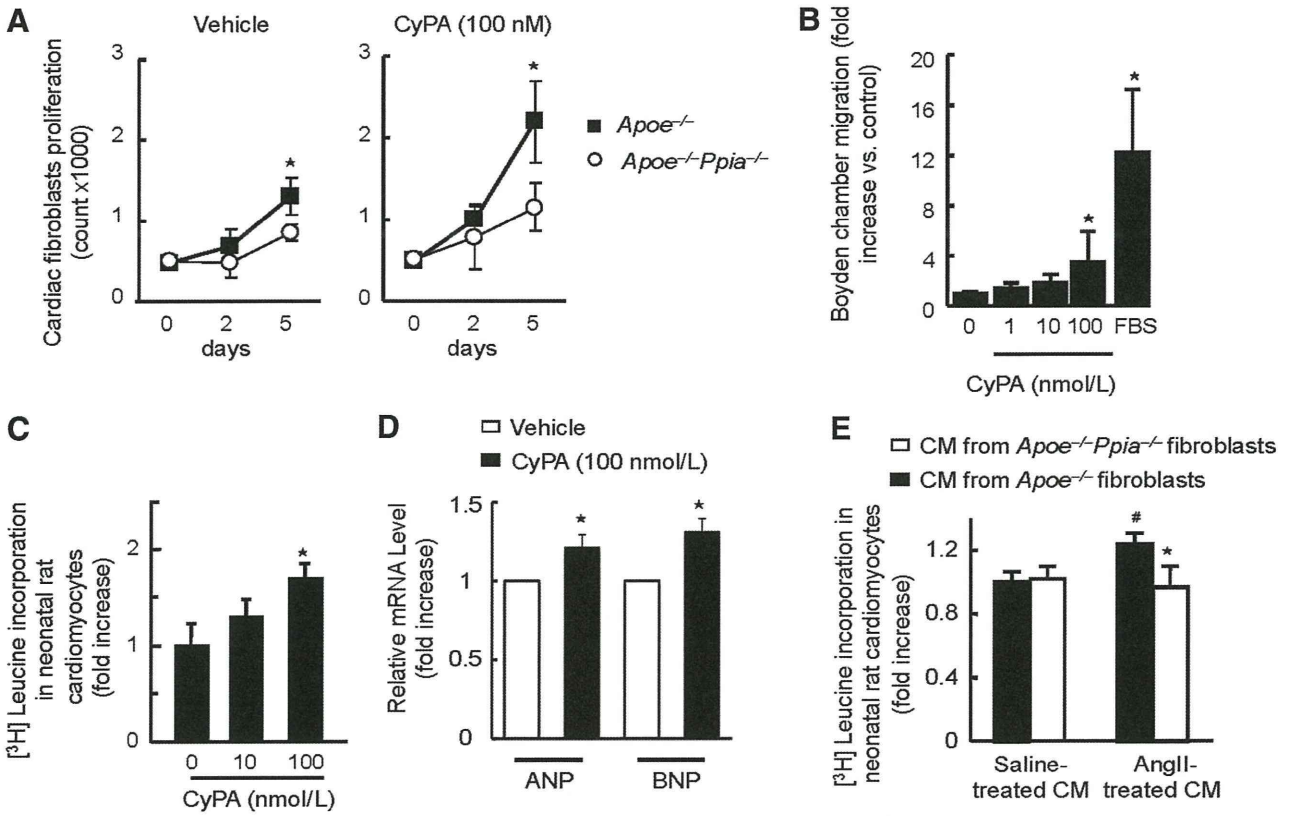

Figure 6. CyPA promotes proliferation and migration of cardiac fibroblasts and hypertrophy of cardiac myocytes. A, After starvation for 24 hours, cardiac fibroblasts from *Apoe*$^{-/-}$ and *Apoe*$^{-/-}$*Ppia*$^{-/-}$ mice were stimulated with 100 nmol/L CyPA or vehicle for 5 days. Medium was changed at day 2, and cells were counted at days 2 and 5. Data are mean±SD. *P<0.01. n=4 in each group. B, Recombinant CyPA promotes cardiac fibroblasts migration in a dose-dependent manner. Data are mean±SD. *P<0.01 compared with control. n=6 in each group. C and D, Neonatal rat cardiac myocytes were treated with recombinant CyPA (0, 10, 100 nmol/L) for 24 hours. Hypertrophy was assessed by the [^{3}H]leucine incorporation method (C) and by measuring atrial natriuretic peptide and brain natriuretic peptide mRNA levels (D). Results are mean±SD. *P<0.05. E, Cardiac myocytes were stimulated with CM prepared from cardiac fibroblasts that were treated with saline or Ang II for 12 hours. Hypertrophy of neonatal rat cardiac myocytes was determined by means of [^{3}H]leucine incorporation. Data were normalized to myocytes stimulated by CM prepared from saline-treated *Apoe*$^{-/-}$ fibroblasts. n=9 in each group. Results are mean±SD. #P<0.05 in saline treated CM vs Ang II; *P<0.05 in *Apoe*$^{-/-}$ vs *Apoe*$^{-/-}$*Ppia*$^{-/-}$ CM.

cardiac hypertrophy (Supplemental Figure III): (1) CyPA is a key determinant for ROS generation, (2) secretion of CyPA in the *Apoe*$^{-/-}$ background is characterized by increased oxidative stress and inflammation, (3) CyPA has a direct hypertrophic effect on cardiac myocytes, and (4) CyPA stimulates proliferation of cardiac fibroblasts that also secrete CyPA, which indirectly stimulates cardiac myocyte hypertrophy. Together, these direct and indirect effects of CyPA contribute to cardiac hypertrophy in *Apoe*$^{-/-}$ mice in response to Ang II.

To examine the involvement of CyPA in the process of the cardiac hypertrophy, we used the Ang II–infusion approach, a well-established mouse model by which to study cardiac hypertrophy. Here, we observed no significant differences in the magnitude of the hypertrophy induced by Ang II between WT and *Ppia*$^{-/-}$ mice on a C57Bl/6 background. Therefore, we investigated the effect of CyPA in *Apoe*$^{-/-}$ mice because they are characterized by high ROS and inflammation.[27] We have recently shown that extracellular CyPA promotes vascular ROS production, which will further induce CyPA secretion and enhance ROS generation.[11] The fact that the CyPA effect was most apparent in the setting of *Apoe* deficiency supports our concept that CyPA plays a key role under conditions in which ROS production contributes to cardiac hypertrophy. However, it is also conceivable that the hyperlipidemia or heightened inflammation characteristic of this model could have contributed to the observed effects.

We anticipated that the *Apoe*$^{-/-}$ background would greatly exacerbate the CyPA-mediated hypertrophic response because Ang II–induced CyPA secretion is significantly elevated in these mice.[11] Consistent with this concept, we found that CyPA secretion from cardiac fibroblasts isolated from WT mice was dramatically lower compared with *Apoe*$^{-/-}$ fibroblasts when stimulated with Ang II.

CyPA has important roles in the immune system and is a well-described regulator of T-lymphocyte functions.[28] It is relevant to note that the primary sources of CyPA responsible for cardiac hypertrophy are likely cells in the heart and not inflammatory cells, because transplantation with *Ppia*$^{+/+}$ bone marrow cells still resulted in less cardiac hypertrophy in *Apoe*$^{-/-}$*Ppia*$^{-/-}$ compared with *Apoe*$^{-/-}$ mice (Figure 4). In addition, transplantation of *Apoe*$^{-/-}$*Ppia*$^{-/-}$ bone marrow into *Apoe*$^{-/-}$ did not prevent cardiac hypertrophy in response to Ang II (Figure 4H). These data suggest the importance of cardiac-derived CyPA for recruitment of bone marrow–derived cells to perivascular tissues to create an environment that is prohypertrophic.